THEORETICAL INVESTIGATION OF CARBON NANOTUBE DEVICES FOR MILLIMETER/SUBMILLIMETER WAVE ANALOG CIRCUITS

by

Josephine Anne Daggett

A thesis submitted in partial fulfillment
of the requirements for the degree

of

Master of Science

in

Electrical Engineering

MONTANA STATE UNIVERSITY
Bozeman, Montana

December, 2009

APPROVAL

of a thesis submitted by

Josephine Anne Daggett

This thesis has been read by each member of the thesis committee and has been found to be satisfactory regarding content, English usage, format, citation, bibliographic style, and consistency, and is ready for submission to the Division of Graduate Education.

Dr. James P. Becker

Approved for the Department of Electrical and Computer Engineering

Dr. Robert C. Maher

Approved for the Division of Graduate Education

Dr. Carl A. Fox

STATEMENT OF PERMISSION TO USE

In presenting this thesis in partial fulfillment of the requirements for a master's degree at Montana State University, I agree that the Library shall make it available to borrowers under rules of the Library.

If I have indicated my intention to copyright this thesis by including a copyright notice page, copying is allowable only for scholarly purposes, consistent with "fair use" as prescribed in the U.S. Copyright Law. Requests for permission for extended quotation from or reproduction of this thesis in whole or in parts may be granted only by the copyright holder.

Josephine Anne Daggett

December, 2009

DEDICATION

This thesis is dedicated to everyone who has contributed and been a part of enriching my education over the years and encouraged me along the way, most of all my parents.

ACKNOWLEDGEMENTS

I would like to first acknowledge and thank my adviser, Dr. James Becker, for giving me the opportunity to work on this project and continue with my education over the past two years. Thank you for your irreplaceable guidance throughout the process. Your commitment to your students and enthusiasm for teaching is not lost on any who have had the opportunity to work with you. I would also like to thank my committee members, Dr. Todd Kaiser and Dr. Yves Idzerda, for their comments and suggestions to further improve this thesis. The feedback you provided is greatly appreciated. Finally and most notably, I thank my family for their unwavering support and encouragement throughout the years.

TABLE OF CONTENTS

TABLE OF CONTENTS – CONTINUED

LIST OF TABLES

LIST OF TABLES – CONTINUED

LIST OF FIGURES

LIST OF FIGURES – CONTINUED

LIST OF FIGURES – CONTINUED

LIST OF FIGURES – CONTINUED

LIST OF FIGURES – CONTINUED

ABSTRACT

Carbon nanotubes have become a very exciting area of research in the field of nanoelectronics in the past few years. Diodes and transistors fabricated using carbon nanotubes are theoretically very promising. Although, experimentally these devices are challenging to successfully realize it is hoped that further research and improvements in fabrication procedures will yield devices which could match or surpass current CMOS technologies. However, there are still many areas that need to be improved before anyone sees these devices mass produced commercially. This thesis gives a detailed overview of the fundamentals of these devices which can be easily understood by someone with a typical electrical engineering background. The purpose of this thesis is to investigate both the theory behind these devices and to conduct a series of simulations in order to determine how they compare to ultimately scaled CMOS for high frequency applications by ignoring the challenges associated with fabricating these devices reliably. In other words, at best how could these devices perform if they could be mass produced with high yield compared to current technologies?

First an introduction to carbon nanotubes and a review of relevant concepts from solid-state electronics will be given, followed by a brief overview of quantum theory for 1-D systems as it pertains to nanotube based electronics. This will then be used to develop models for a Schottky diode and Schottky barrier transistor. Simulations using these models were conducted that show the potential for these devices for high frequency electronics. These results are subsequently used to compare to current state-of-the-art technologies. Upon completion of the simulations in this thesis, it was determined that carbon nanotube based Schottky diodes and Schottky barrier transistors do not perform as well as current technologies in relation to applications for submillimeter/millimeter wave detection and analog circuits, even when assuming no limitations imposed due to poor fabrication.

INTRODUCTION TO CARBON NANOTUBES AND REVIEW OF RELEVANT CONCEPTS FROM SOLID-STATE ELECTRONICS

Overview

Since the development of complementary metal oxide semiconductor (CMOS) circuits in 1963 there have been great strides towards scaling devices down to smaller and smaller dimensions along with better performance and production efficiency. However, in recent years it has become apparent that the ultimate end may be approaching, the ability to scale devices down further is reaching its limit. For this reason researchers are delving into the world of nanotechnology to investigate the ability of nano-devices in replacing ultimately scaled CMOS. At present, most nano-devices have exhibited poor characteristics and unreliable manufacturing processes and thus do not pose a serious threat to replacing CMOS in the near future.

One of the more promising nanoelectronic materials is the carbon nanotube (CNT). Carbon nanotubes are frequently reported as being discovered in 1991 by Iijima, who was studying the soot produced after vaporizing graphite and subsequently published an influential paper on his discovery [1]. However, the story around the discovery of CNTs is much more complex and there are other individuals who have contributed toward their discovery prior to Iijima [1]. CNTs exhibit excellent electrical properties due to their small size and structural purity resulting in ballistic transport behavior, meaning that it is possible to achieve high electrical conductivity with no loss due to scattering. Theoretically, carbon nanotube based electronics should be capable of operating at very high frequencies, opening the door for applications in

millimeter/submillimeter nanoelectronics. Currently there are significant challenges in creating reliable and cost-effective CNT-based devices even if they are found to exhibit excellent high-frequency performance. One of the biggest difficulties is establishing good electrical contact to nanotubes that does not hinder the operation of a device. Later it will be shown that CNTs exhibit high contact resistance due to their 1-dimensinal nature and small contact area (the contact resistance is inversely proportional to the contact area). This large resistance makes it difficult to achieve the desirable operating frequency as per millimeter/submillimeter wave devices and also creates challenges for effective power delivery.

After completing a comprehensive search of the literature regarding CNTs and their prospects for future applications in nanoelectronics, there appears to be an absence of a detailed overview, from a single source, of the fundamental quantum physics behind CNTs that can be easily understood by someone with a typical electrical engineering background. Furthermore, a significant portion of the published experimental data is in many cases incomplete if not contradictory. Although theoretically, CNT based devices for high frequency electronics are promising, there is a need to investigate collectively both theoretical interpretations and simulated results in order to determine how plausible these devices are in comparison to ultimately scaled CMOS (this is particularly true for high frequency applications).

The main objective of this work is to analyze the potential advantages and disadvantages that CNT devices have in comparison to ultimately scaled CMOS for

millimeter/submillimeter wave analog circuits. This will be accomplished by completing the following:

- Review the basic material and electrical properties of CNTs.
- Give an overview of the quantum theory that is relevant to the study of CNT devices.
- Establish equivalent circuit models for a CNT based diode and MOSFET, in which model parameters are based on a combination of quantum concepts and published experimental results.
- Use the models to simulate the performance of a submillimeter wave diode detector and small-signal amplifier.
- Summarize information gleaned from simulations and pertinent publications to assess the challenges associated with obtaining CNT devices that are competitive with ultimately scaled CMOS for high frequency electronics.

This chapter will discuss the basic structure of a CNT, its electrical properties, the operation of devices beginning with a review of basic semiconductor physics, and the methods for producing CNTs. It will also explain the structure and operation of CNTFETs (Carbon Nanotube Field-Effect Transistors) and diodes with particular emphasis on their prospects for high-frequency applications. The second chapter will discuss the quantum theory behind the transport in 1-dimensional systems and how it relates to CNTs, which will lead into a theoretical analysis of a CNT-based Schottky diode and Schottky barrier FET equivalent circuit model.

Molecular Structure of CNTs

There are two different categories of CNTs, multi-walled (MWCNTs) which consist of two or more layers of concentric graphite cylinders having outer diameters typically ~ 2.5-30nm and single-walled (SWCNTs) made of only one cylinder of graphite [2]. Single-walled CNTs have diameters as low as ~1nm and in general are the ones which have been used for creating carbon nanotube based electronic devices. Currently, the electronic properties of MWCNTs are not as well known as SWCNTs, but it has been reported [3] that by collapsing and thus deforming the structure of a MWCNT one can utilize them for making CNTFETs. There are also other reports in the field of electronics and optics demonstrating successful multi-walled CNT based devices.

The electronic structure of carbon nanotubes is purely dependent upon their physical structure (chirality and diameter) which is unique when compared to other materials. Therefore, in order to analyze the electronic properties of SWCNTs it is essential that we first understand the structure of CNTs, which is defined by their diameter and chirality. The chirality of a nanotube is characterized by the coefficients (n, m) of the chiral vector, where $0 \le m \le n$ with m=n=0 being degenerate. This vector is determined by unrolling the SWCNT into a 2D sheet that will have the same lattice structure of a single layer of graphite in 2D (graphene). A chiral vector map of SWCNTs is illustrated in Fig. 1.1, where the chiral vector is defined as

$$\vec{C} = n\vec{a}_1 + m\vec{a}_2 . \qquad (1.1)$$

The vectors $\vec{a}_1$ and $\vec{a}_2$ are the unit cell base vectors of the unrolled 2D sheet (graphene) and have a magnitude of 0.246nm [2]. As given in (1.2), the magnitude of the chiral

vector $\vec{C}$ in nanometers can be determined by knowing the coefficients (n,m) and that the carbon bond length, $a_{c\text{-}c}$ = 0.142 nm. The diameter can be determined by equation (1.3) due to the fact that the chiral vector describes the circumference of the nanotube. With just these two simple equations it is possible to determine the band gap, inherent capacitances and inductance of a SWNT, and whether a SWNT will be metallic or semiconducting.

$$|\vec{C}| = a_{c-c}\sqrt{3}\sqrt{(n^2 + nm + m^2)} \tag{1.2}$$

$$Diameter = \frac{a_{c-c}\sqrt{3}\sqrt{(n^2 + nm + m^2)}}{\pi} \tag{1.3}$$

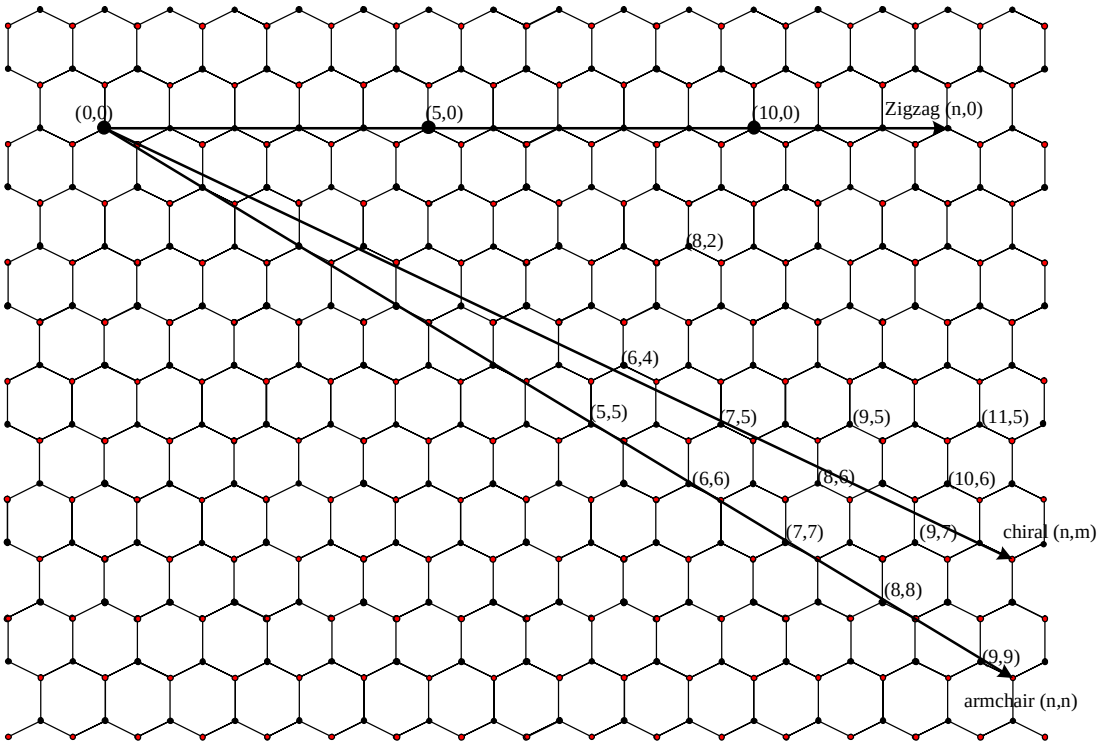

Figure 1.1: Chiral vector map for carbon nanotubes [4].

The two structures that are symmetrical, illustrated in Fig. 1.1 by the two outer chiral vectors, are known as zigzag and armchair nanotubes, however it is currently believed that most are chiral having structures lying somewhere between these two. For zigzag nanotubes, either the coefficient m=0 with n being any integer value greater than or equal to one (n,0), or n=0 with m being any integer value greater than or equal to one (0,m). The armchair structures occur when the two coefficients equal one another, n=m. After rolling the graphene sheet into a cylinder, the carbon nanotube will resemble one of the three possible structures illustrated in Fig. 1.2 distinguished by the values of n and m.

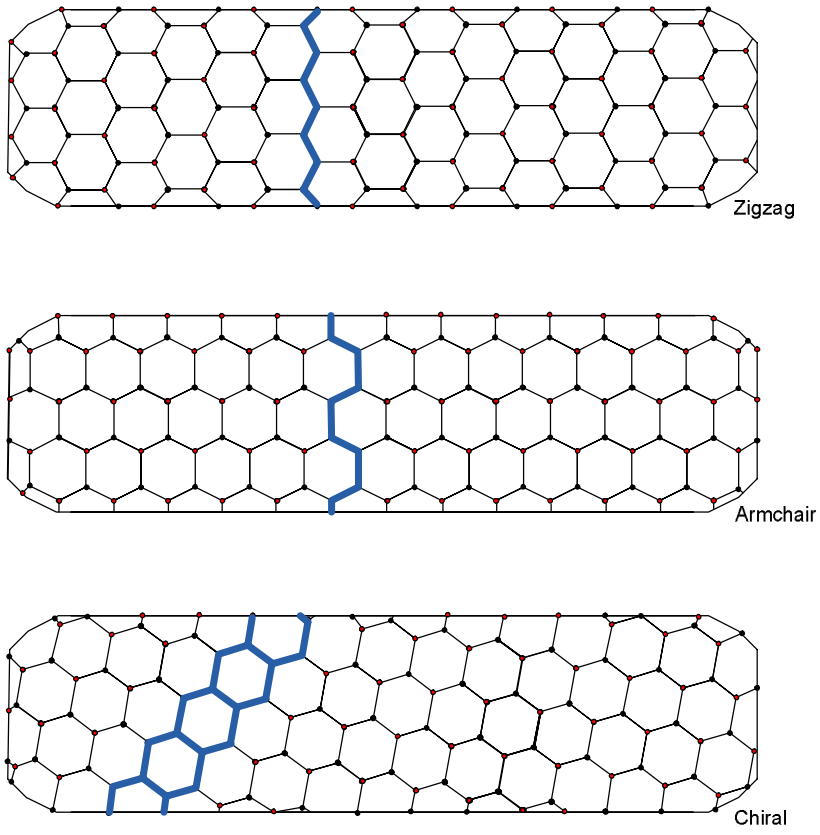

Figure 1.2: Three possible carbon nanotube structures, zigzag (n,0), armchair (n,n), and chiral (n,m) [2].

Electrical Properties of CNTs

As with all materials, in order to understand the electrical properties of CNTs we will need to examine their electronic band structure and the factors that determine whether they are metallic or semiconducting. As mentioned in the previous section this can be determined by knowing the chirality coefficients, but we have not yet shown how they can tell us this information. This will be explained next along with a brief overview of the existing methods used for growing CNTs. Later in Chapter 2 we will return to this topic and analyze it in more detail by the means of a quantum mechanical perspective.

Band Structure

The electronic band structure of a semiconductor consists of a valence band, conduction band, and Fermi level that are at energy levels particular to a given semiconductor. The Fermi level is the energy of the highest occupied state of electrons at absolute zero, and the valence band contains the valence electrons that when excited can move to the higher energy levels of the conduction band. If a potential is applied across the contacts to a semiconductor and enough energy has been imparted to the electrons such that they are raised to the conduction band, resulting in a state of non-equilibrium, the excited electrons will move in the direction opposite to the applied electric field in an effort to obtain equilibrium. The excitation of the electrons can be accompanied by the formation of holes in the valence band that will travel in the same direction as the applied electric field. Therefore, the overall conductivity of a semiconductor is dependent upon

the concentration and movement of both electrons (in the conduction band) and holes (in the valance band).

Semiconductors are divided into three types, intrinsic, n-type and p-type. In the intrinsic case, the number of free electrons is identical to the number of holes. The operation of a semiconductor is described as n-type when there is a higher concentration of electrons in the conduction band than the intrinsic value, meaning that there will be more electrons in the conduction band than holes in the valence band. For p-type semiconductors the opposite is true, there is an excess of holes in the valence band resulting in a larger concentration of holes than electrons. For n-type the Fermi-level is closer to the conduction band and for p-type it is closer to the valence band. By introducing impurities into the semiconductor through n-type doping or p-type doping one can control the manner of operation. For carbon nanotubes it has been difficult to unambiguously determine their intrinsic properties, but some success has been made towards this endeavor by a thermoelectric power measurement as reported in [5], which concluded that CNTs are p-type when exposed to oxygen and are n-type after vacuum annealing. One of the challenges regarding CNTs has been differentiating between alterations of the Fermi level via their interaction with oxygen and the changes in the metal-CNT contact (Schottky) due to oxygen exposure. What is nice about the thermoelectric power measurement is that it is independent of the CNT-metal contact. Thus, we are able to conclude experimentally that the CNT itself will be p-type when exposed to oxygen, however, it is important to note in order to determine the overall

behavior of a CNT-based device it is essential to also understand the behavior of the CNT-metal contact.

As mentioned earlier, the electronic properties and thus the band structure of carbon nanotubes is dependent upon the diameter and chirality of the tubes. Later when building a model for a CNT Schottky diode it will become obvious that determining the Fermi energy will be necessary for estimating the inductance and capacitance of a given carbon nanotube. Methods of modulating the Fermi energy include doping the nanotube with acceptors in order to lower the Fermi level (p-type) or with donors to raise the Fermi level (n-type) and as a result change the behavior of a CNT-based device. Most of the doping for CNTs has been reported as interstitial with O_2, I_2, NO_2, and Br_2 acting as acceptors and Cs, NH_3, and K as donors [5].

The band gap E_g, which is the energy difference between the bottom of the conduction band and the top of the valence band, is inversely proportional to the diameter of the carbon nanotube.

$$E_g \propto \frac{1}{d} \tag{1.5}$$

The work function, which is the energy required to move an electron from the Fermi level to the vacuum level, of SWNT is also dependent upon the diameter of the CNT, however the relationship is more complex. Figure 1.3 on the following page shows metallic and semiconducting tubes with various chirality coefficients in relation to their work function and diameter. It is clear that the operation of CNT-based devices will be strongly dependent upon the diameter, chirality, and the choice of metal contacts made to the CNT.

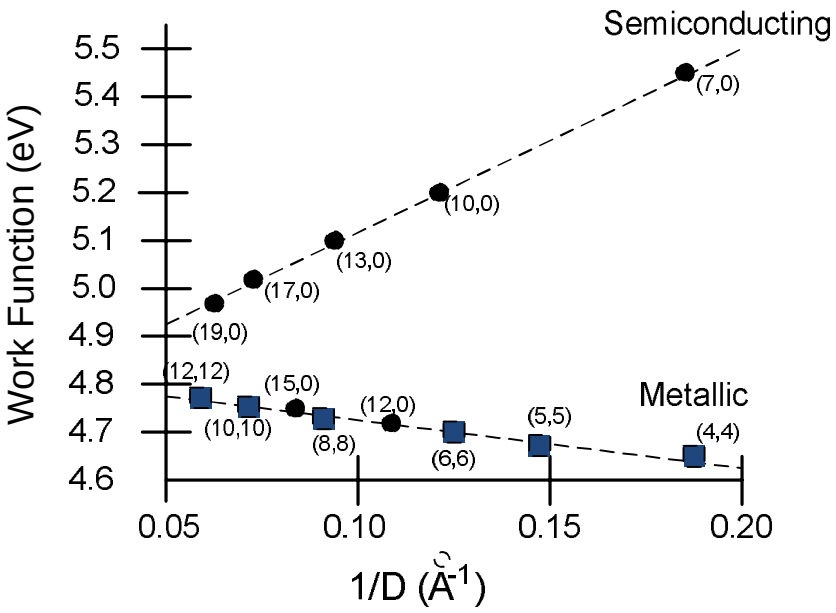

Figure 1.3: Work functions of SWNTs vs. inverse of tube diameter (squares = armchair, circles = zigzag) from [6].

Metallic and Semiconducting CNTs

The chirality of a carbon nanotube determines whether it will be metallic or semiconducting. It has been shown by [7] and [8] that CNTs will be metallic when n-m is a multiple of 3,

$$n - m = 3q \tag{1.6}$$

where n and m are the chiral vector coefficients and q is an integer (the relationship of equation 1.6 will be derived in Chapter 2). All armchair SWCNTs are metallic, while zigzag tubes will be metallic when n is a multiple of 3. Therefore, approximately $\frac{1}{3}$ of carbon nanotubes will be metallic and $\frac{2}{3}$ semiconducting based upon equation (1.6),

assuming equally diverse values for n, m, and q. Most reports on the growth of CNTs have verified this [2].

Synthesis of CNTs

Carbon nanotubes can be developed by laser ablation, arc discharge of graphite, or chemical vapor deposition (CVD). The arc discharge method of growing CNTs is the cheapest and easiest way to create large quantities, but typically the CNTs produced by this method have more defects than those produced through laser ablation processes [5]. Alternatively, the laser ablation technique is not suitable for growing large quantities of carbon nanotubes. Therefore, in the future if the incorporation of CNTs into nanoelectronics proves to be viable, it will be necessary to develop a robust and controllable process for large scale production, thus the laser ablation method will probably be surpassed by others that can effectively produce for bulk applications, the most probable being CVD.

In order for CNTs to be used for nanoelectronic applications it is desirable to have CNTs grown on substrates with reasonable control. Chemical vapor deposition (CVD) is used as a reliable way to grow CNTs on substrates with controllable growth rates, diameters, and lengths. CVD has also been an excellent way of growing several pure nanotubes of relatively the same diameter and alignment [9], allowing numerous CNTs to be used in parallel to decrease the high resistance associated with one-dimensional systems. This method uses methane, carbon monoxide, acetylene, or evaporated ethanol as a carbon source that is then defused onto the substrate (typically silicon or quartz) and

attaches itself to a catalyst that was heated onto the substrate. The choice of catalyst can affect whether the CNTs produced will tend to be SWCNTs or MWCNTs (typical catalysts include Ni, Fe, Mo, and Co) [5]. Figures 1.4 and 1.5 depict the CVD process flows for two recipes that have been found to realize SWCNTs.

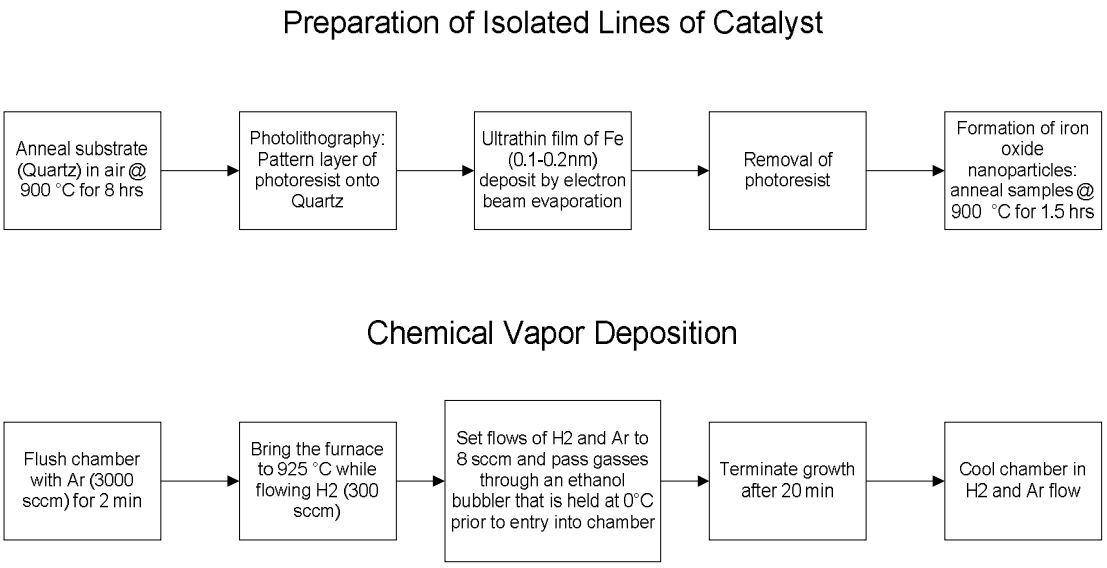

Figure 1.4: CVD process using evaporated ethanol [9].

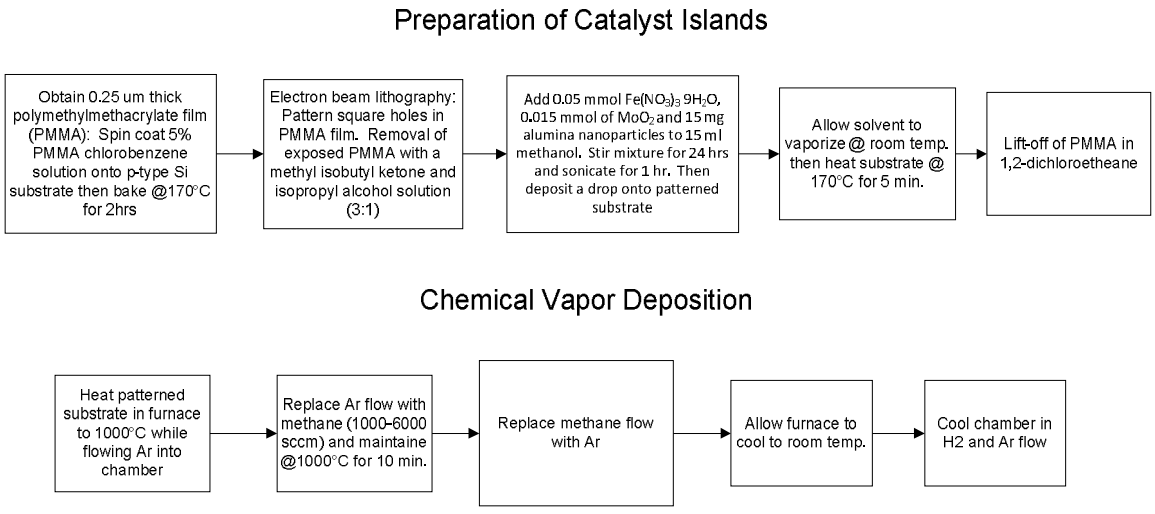

Figure 1.5: CVD process using methane [10].

No matter the method used for growing nanotubes, there will be defects and impurities found in the CNTs. Currently there are a number of methods available including thermal oxidation in air and acid oxidation that remove some of these impurities [5]. Thermal annealing after the metal electrodes have been deposited on top of the CNT is often used to significantly reduce the contact resistance at the metal-CNT junction. Determining ways of improving the contacts and purity of CNTs are two of the most essential aspects regarding the future development of CNT-based electronics.

Carbon Nanotube based Devices

CNT Schottky Diodes

Schottky diodes play an important role in high frequency electronic applications as sensors, frequency multipliers, and mixers because of their fast switching speeds, inherent high current carrying capacity, and low forward voltage drop. Semiconducting nanotubes appear to be promising for the use in Schottky diodes with cut-off frequencies predicted in the THz range [11]. This section will discuss the operation of a Schottky diode (one contact being ohmic and the other Schottky) by examining several band diagrams covering both before and after the metal and CNT make contact.

First we will analyze what occurs when a metal makes contact to a semiconductor (CNT) and the semiconductor is n-type (recalling that CNTs are generally p-type as a result of the exposure to oxygen in air) and the work function of the metal is greater than the work function of the semiconductor, thus creating a Schottky contact. We will continue and consider the case in which the semiconductor is p-type and ultimately

discuss ohmic contacts and a means of mitigating the high contact resistance associated with CNT-devices.

The amount of energy that is necessary in releasing an electron at the Fermi level from the metal is equal to the value of the work function $q\Phi_m$. While the metal and CNT are separated, the energy band diagram resembles Figure 1.6. For this case, the work function of the metal is greater than the work function of the n-type CNT, $\Phi_m > \Phi_{CNT}$. Therefore, the CNT Fermi level is higher than the Fermi level of the metal before contact. After the metal approaches and makes contact with the nanotube having a work function $q\Phi_{CNT}$, the Fermi levels become aligned, reaching equilibrium (Figure 1.7). In order for equilibrium to occur, the Fermi level of the CNT must be lowered relative to that of the metal by an amount equal to $\Phi_m - \Phi_{CNT}$. A contact potential, V_O is created between the metal and CNT due to the creation of an electron depleted region having width *W*. This region is created because the electrons from the CNT move into lower energy levels and accumulate near the surface of the metal as shown in Figure 1.7 [12] and [13]. The electrons that move to a lower energy state leave behind excess holes, or a net positive charge. Eventually, equilibrium will occur and the net flow of electrons from the CNT to the metal will cease. A barrier is formed between the metal and semiconductor, called the Schottky barrier, which prevents electrons from moving to the semiconductor from the metal. This barrier has a height Φ_B and is equal to the difference between the work function of the metal and the electron affinity χ as illustrated in Figure 1.7 and given in (1.11).

$$q\phi_B = q(\phi_m - \chi) \tag{1.11}$$

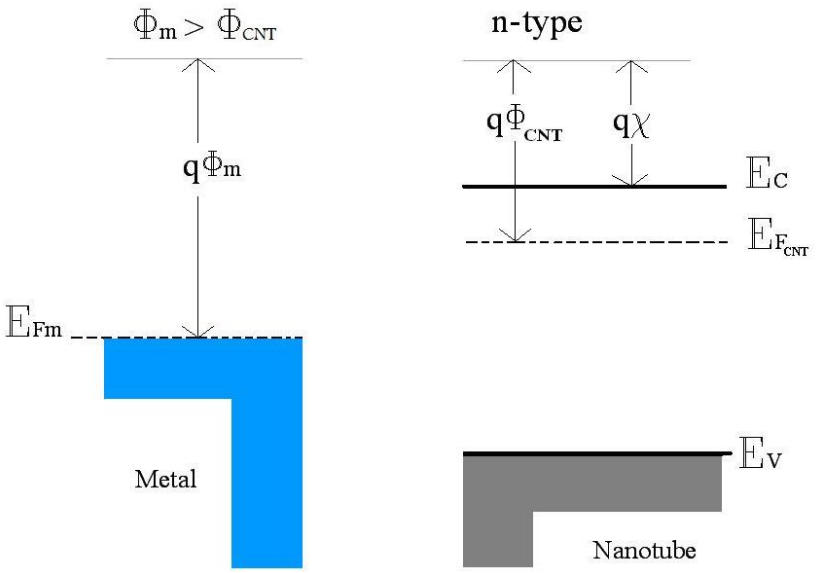

Figure 1.6: Energy band diagram before making contact when CNT is n-type ($\Phi_m > \Phi_{CNT}$).

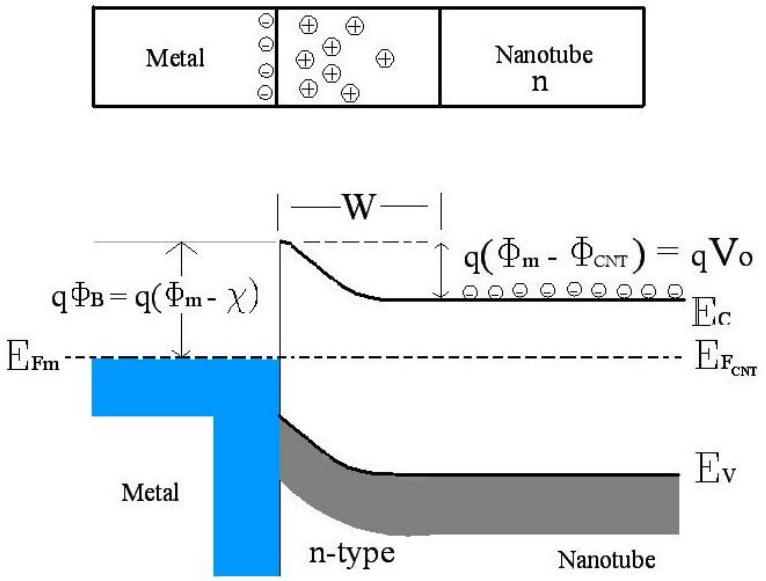

Figure 1.7: Energy band diagram after making contact (equilibrium) with n-type CNT ($\Phi_m > \Phi_{CNT}$).

There will be no net current conduction through the junction under zero bias conditions. However, if a sufficiently large positive voltage is applied to the metal side, such that V_O is reduced until it is possible for electrons from the conduction band of the CNT to overcome the reduced barrier, current can flow between the metal-CNT junction (Figure 1.8).

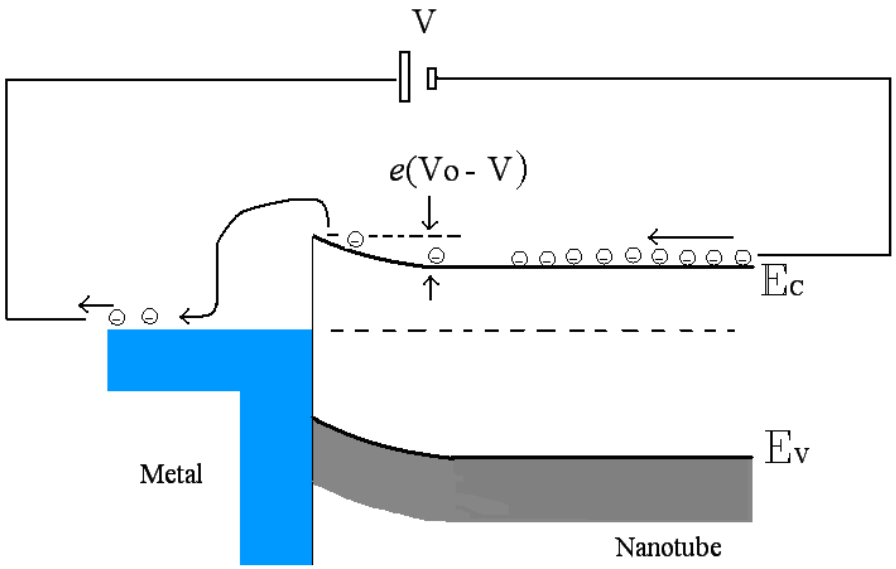

Figure 1.8: Forward-biased metal-CNT junction when the CNT is n-type ($\Phi_m > \Phi_{CNT}$).

Conversely, when the Schottky barrier is reverse-biased (Figure 1.9), V_O is increased making it extremely difficult for the electrons in the CNT to overcome the barrier and move into the metal. Under these conditions there is virtually no current flow, and any amount present is mostly due to thermal emission of electrons over the barrier from the metal to the conduction band of the CNT. Combined, the bias conditions reveal the current-voltage characteristic of a diode.

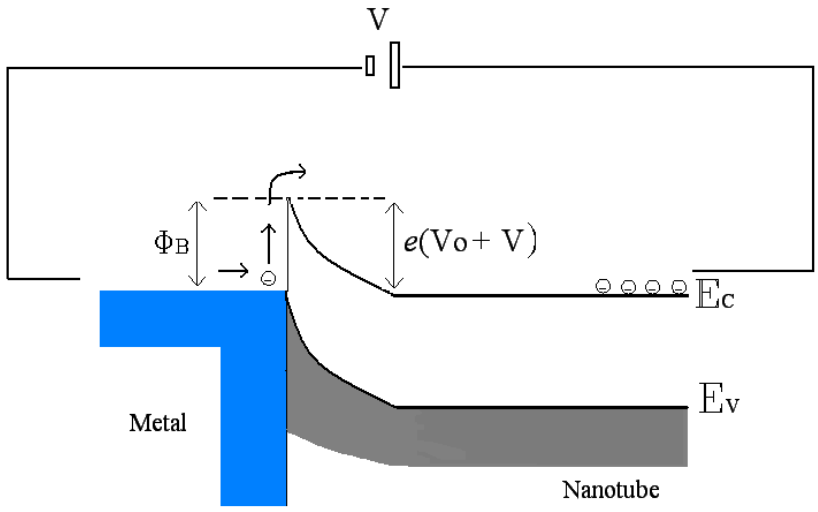

Figure 1.9 Reverse-biased metal-CNT junction when the CNT is n-type ($\Phi_m > \Phi_{CNT}$).

Now we will discuss the case when the work function of the metal is less than that of the CNT and the CNT is p-type. For this instance the Fermi level of the metal is higher than that of the CNT. As before, when the two are brought together and contact is made, charge transfer will occur until the Fermi levels align and thermal equilibrium is established. However, we are now interested in the transfer of electrons from the metal to the CNT. This time an excess positive charge accumulates on the metal side of the junction and a net negative charge forms on the CNT side. The depletion region W is formed and as before there is a potential V_O across it. A Schottky barrier with height Φ_B is formed at the junction that prevents electron diffusion from the metal to the CNT. The barrier height for the p-type CNT is given by (1.12)

$$q\phi_B = E_g - q(\phi_m - \chi)\,. \tag{1.12}$$

E_g is the band gap, which is equal to the energy difference between the lowest energy level in the conduction band and the highest level in the valence band. The energy band diagram of before making contact when the CNT is p-type is shown below (Figure 1.10).

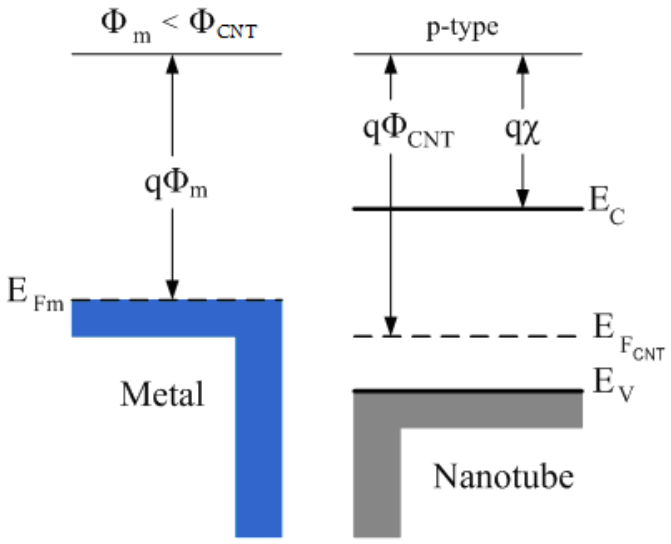

Figure 1.10: Energy band diagram before making contact when CNT is p-type ($\Phi_m < \Phi_{CNT}$).

Additionally, the energy band diagram of after making contact (equilibrium) with a p-type CNT is depicted in Figure 1.11.

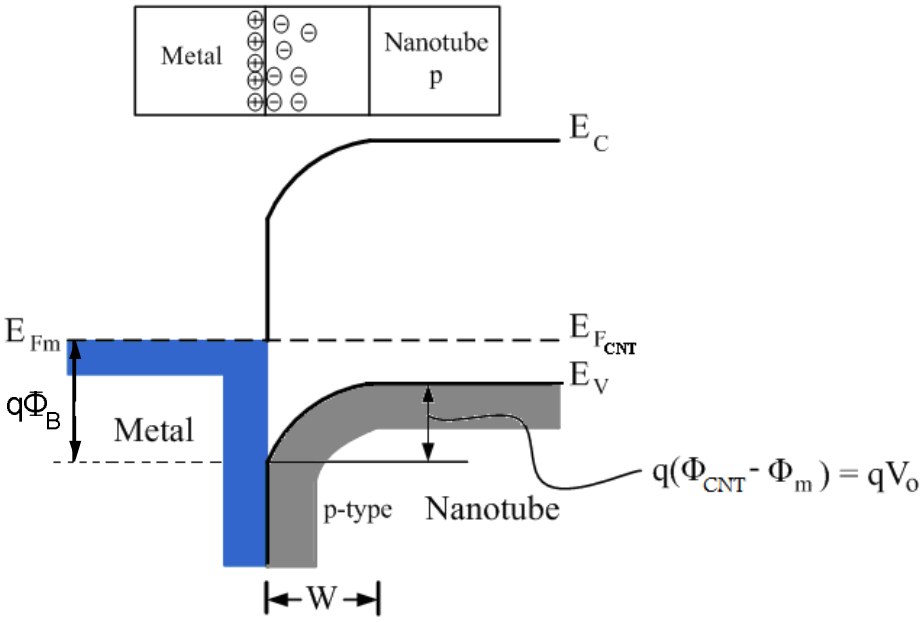

Figure 1.11 Energy band diagram after making contact (equilibrium) with p-type CNT ($\Phi_m < \Phi_{CNT}$).

The barrier can be lowered to allow the transfer of electrons from the metal into the CNT by applying a negative voltage V to the metal rather than the positive voltage applied previously for the metal/n-type CNT Schottky junction (Figure 1.12). Conversely, the junction is reverse biased when a positive voltage is applied across it from metal to semiconductor (Figure 1.13).

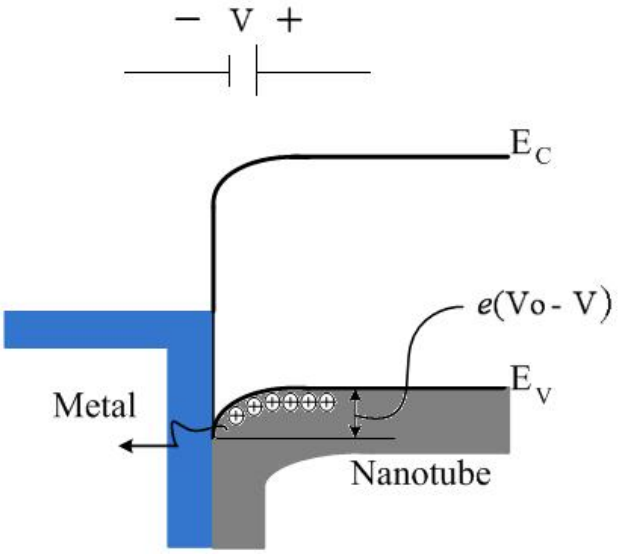

Figure 1.12: Forward-biased metal-CNT junction when the CNT is p-type ($\Phi_m < \Phi_{CNT}$). Current is comprised of electrons moving from the metal to the CNT.

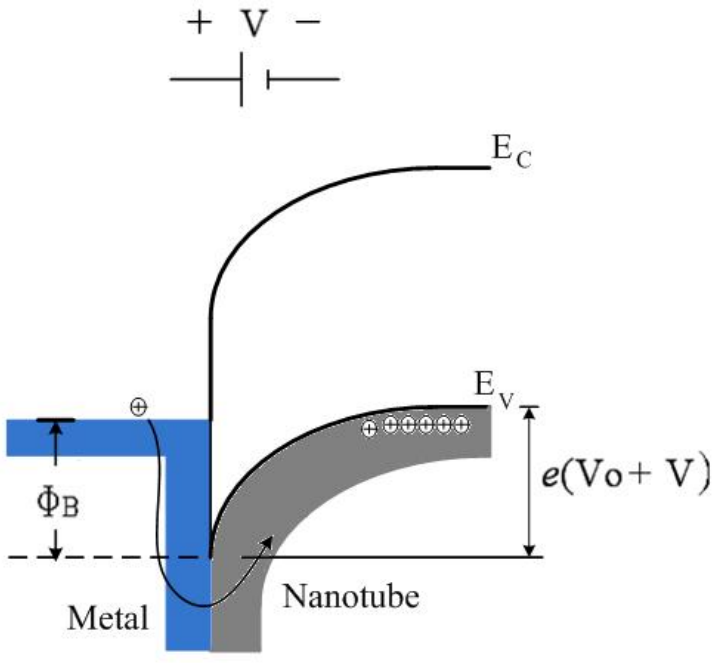

Figure 1.13: Reverse-biased metal-CNT junction when the CNT is p-type ($\Phi_m < \Phi_{CNT}$). What little reverse current that flows under this condition is comprised of electrons traveling from the CNT to the metal.

The factor that determines whether the junction between a metal and a semiconductor will exhibit behavior consistent with that of a Schottky contact or an ohmic contact depends on whether the semiconductor is n or p-type and the work function of the metal. When the work function of the metal is sufficiently larger than that of the n-type CNT, the junction will operate as a Schottky contact. In the opposite case, when $\Phi_m < \Phi_{\text{n-CNT}}$ the junction (ideally) would be ohmic (the reverse being true for a p-type CNT). One can see that the work function of the metal contact plays a significant role in the operation of the CNT device by modulating the barrier height. It has been shown [14] that by choosing appropriate metals for contacts and not doping the CNT one can achieve p-type, n-type, and ambipolar characteristics. However, as mentioned several times before, it is extremely difficult to achieve anything close to a perfect contact to the carbon nanotube where the contact does not limit the flow of electrons.

Ohmic Contacts

As mentioned earlier, another important factor to consider is the ability to create an ohmic contact to a CNT, meaning a contact that has a linear I-V relationship in either biasing directions. Ideally the contact will have very low resistance and thus not limit current flow. However, in the case of carbon nanotubes this resistance is fairly large and significantly contributes to the operation of devices. (From now on, for all further discussions one should assume the CNT is p-type unless mentioned otherwise.) It has been established that using palladium or gold results in a Schottky contact, while platinum produces an ohmic contact [15]. Performance can be improved by annealing the electrodes which lowers the detrimentally high contact resistance. Figures 1.14 and

1.15 are the band diagrams before contact and after contact for an ideal ohmic junction for a p-type semiconductor.

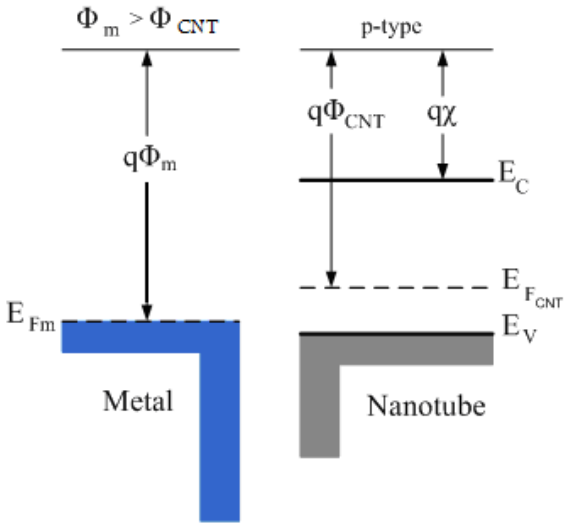

Figure 1.14: Prior to contact between a metal and p-type CNT where $\Phi_m > \Phi_{CNT}$.

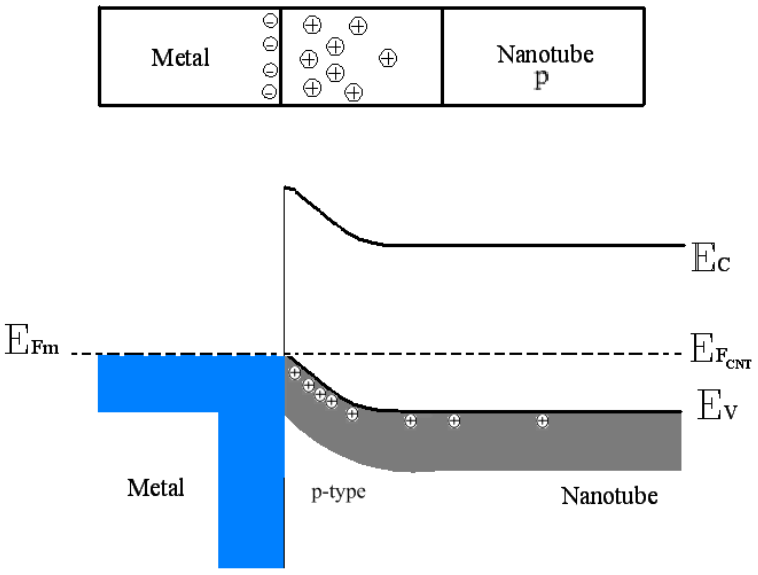

Figure 1.15: After contact between a metal and p-type CNT where $\Phi_m > \Phi_{CNT}$.

CNT PN Junction Diodes

An additional element frequently used in electronics is the P-N diode. A P-N junction diode consists of a p-type semiconductor and n-type semiconductor as illustrated in Figure 1.16 and 1.17. In the case of CNTs, half of the CNT is made n-type while the other half is p-type. This can be accomplished as described in [16] by covering half the CNT with poly (methyl methacrylate) (PMMA)/tetracyanoquinodimethane (TCNQ) producing an enhanced p-type region and the other half with polyethylenimine (PEI) transforming the other half into an n-type region that is stable in air. Such a device is illustrated in Figure 1.18.

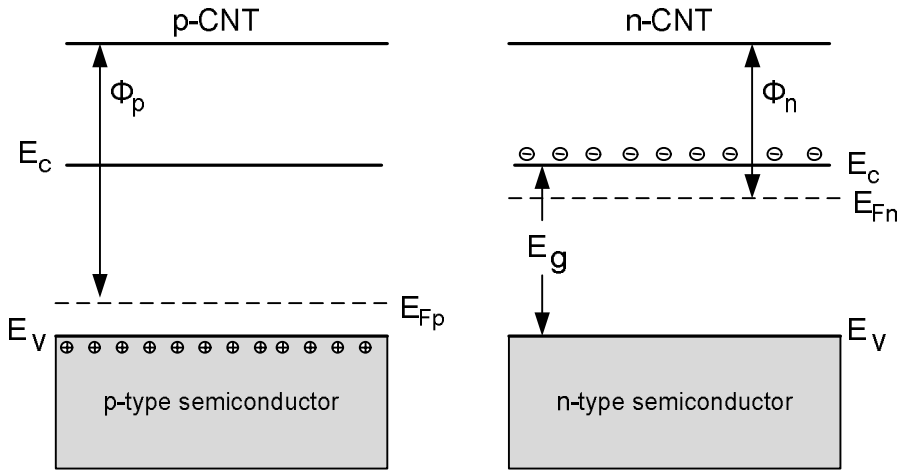

Figure 1.16: P-type and n-type semiconductors before contact (for CNTs the two regions are always in contact due to being within one single tube).

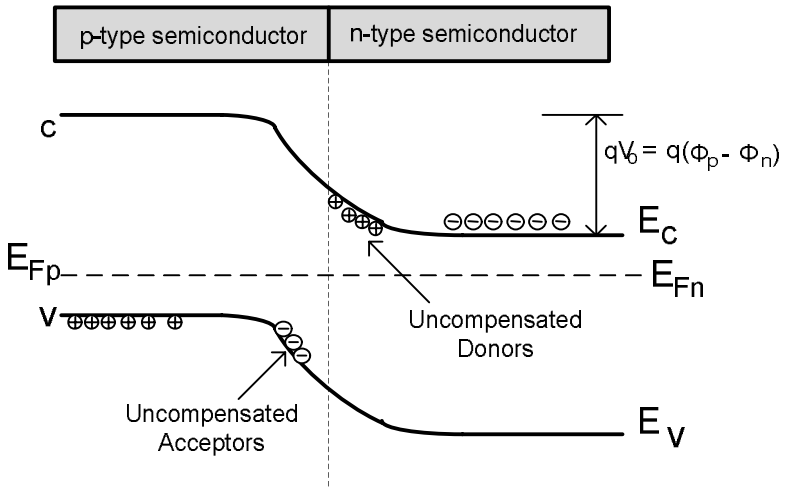

Figure 1.17: PN junction after p-type and n-type semiconductors are brought into contact.

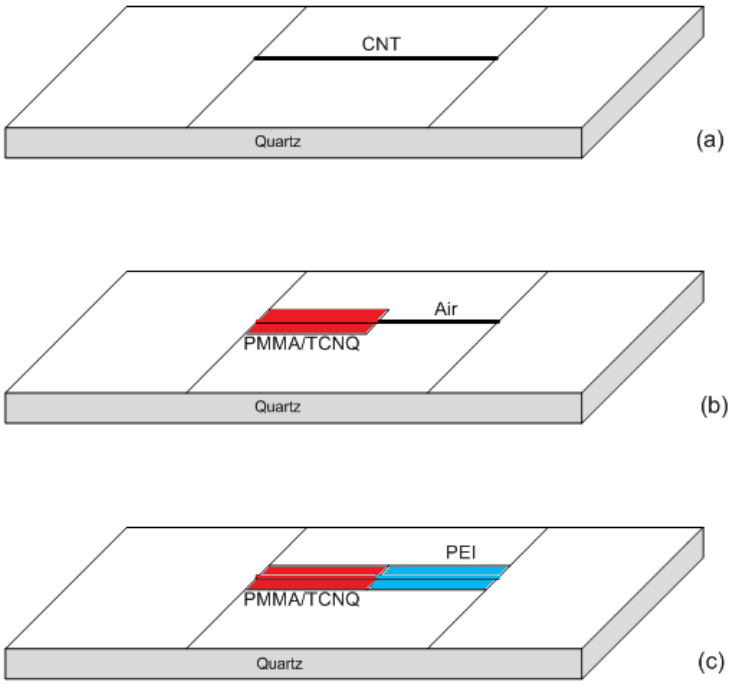

Figure 1.18: (a) CNT before forming p-type and n-type region, (b) CNT after forming enhanced p-type region, (c) CNT after establishing n-type region and thus forming a PN junction [16].

CNT Schottky Barrier Field-Effect Transistor (SBFETs)

Another device that has shown promise besides the Schottky diode and P-N junction diode is the CNT MOSFET. The most common CNTFETs are the Schottky barrier (SB) FETs due to the metal-CNT contact. Because CNTs are p-type when exposed to oxygen these devices are typically p-type, although n-type devices have also been made. The typical structure of a CNT SBFET is shown in Figure 1.19.

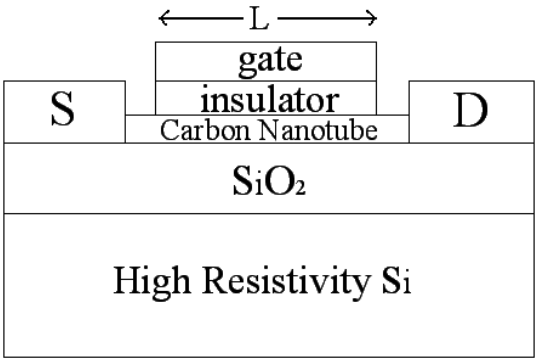

Figure 1.19: CNT Transistor Layout.

The band diagrams from the previous section still apply to the contacts of the CNT-based SBFETs. By creating four gate segments, investigators have been able to confirm ballistic transport in carbon nanotubes as a result of changing the effective channel length between the source and drain and showing that the current does not change as a function of length [17].

Summary

Carbon nanotubes may be considered for future high frequency circuit applications, however it will be more than a few years before this can be realized. At present, there are several areas that need to be investigated including (but not limited to) the following: determining the intrinsic behavior of carbon nanotubes, how to effectively control devices, finding ways to establish better electrical contact to CNTs, improve yield, and finally how to mass produce cost-effective CNT-based electronics. Another reason CNTs are appealing besides direct applications to nanoelectronics, is that they can be studied to verify the Lüttinger model for the transport of interacting electrons in 1-D systems. The results from this model when applied to carbon nanotubes will be used in Chapter 3 to create a model for a Schottky diode and a Schottky FET.

Theoretically, CNTs appear promising, but a more extensive evaluation of how to make these devices reliable and cost-effective needs to be done prior to deciding the future of carbon nanotube based electronics. Also, from the simulations that are reported later in this thesis, CNTs do not appear entirely advantageous with regards to high frequency applications when compared to other materials. However, this does not indicate that they could not be used for other applications in electronics, such as interconnects or thin flexible electronic devices. In the next chapter we will develop the necessary tools to understanding the transport in 1-D systems, which will provide the foundation for our diode and FET models. Following this, we will draw conclusions based upon simulations that demonstrate the behavior of these devises and determine the benefits and challenges associated with CNT-based circuit elements.

QUANTUM THEORY FOR 1-D SYSTEMS

Overview

The purpose of this chapter is to provide a detailed description of the electronic transport in both metallic and semiconducting nanotubes using a quantum mechanical approach. We will begin by returning to the chiral vector map for carbon nanotubes (2-D graphene sheet) discussed in the last chapter and obtain a solution to the Schrödinger equation in a periodic potential for the electrons responsible for conduction near the Fermi energy (the periodicity arises from the crystal structure of the carbon nanotube). This will allow us to determine the energy eigenstates and thus the bandstructure of our system. Two similar methods, the tight binding approximation and Kronig-Penney model will be used to calculate the energy eigenvalues and dispersion relations for graphene, which can be modified slightly for carbon nanotubes by taking into account an extra boundary condition that must be introduced after "rolling" the graphene sheet into a cylinder.

After completing the calculations for these two models (which should yield similar results) it will be clear that there are only two subbands near the Fermi energy. Once spin is taken into account we have the possibility of two electrons (one spin up the other spin down) occupying each subband. Therefore, carbon nanotubes have a total of four modes or "channels" around the Fermi energy that contribute to the overall conductance. There is also a limit imposed on the maximum achievable conductance allowed per mode defined by a fundamental constant that is independent of the length of

the channel. The derivation or origin of this constant will be discussed in order to explain why such a limit exists in a 1-D system even when assuming perfectly transmitted modes and perfect contacts.

The above will be incorporated into our understanding of the electrical properties of metallic and semiconducting nanotubes along with an overview of the possibility of ballistic transport. Finally, at the end of this chapter we will determine the quantum capacitance, electrostatic capacitance, magnetic and kinetic inductance of a single tube and clarify what distinguishes these components from one another. In the following chapter they will be employed in creating a circuit model for a CNT which will be the building block for an RF equivalent circuit of a Schottky diode and Schottky barrier FET. Various simulations involving these equivalent circuits will be conducted in order to illustrate the challenges associated with carbon nanotube based devices for millimeter/submillimeter wave analog circuits.

Tight Binding Model Calculation

The tight binding model will be implemented in this section to calculate the single electron eigenvalues of a 2-D sheet of graphite (a homogenous periodic solid) which can be incorporated into determining the energy levels of the low-dimensional structure of a carbon nanotube. The tight binding model approximates the Hamiltonian of the system based upon a single atom in the lattice and its nearest neighboring atoms. The Hamiltonian is the total operator for the system. In the absence of applied electromagnetic fields, the Hamiltonian may be expressed as

$$H = -\frac{\hbar^2}{2m}\nabla^2 + V(\vec{r},t) \tag{2.1}$$

where $\hbar$ is the reduced Plank's constant and m is the mass of the particle of interest (in our case an electron). Let's begin by describing the unit cell of graphene as containing two carbon atoms as depicted in Figure 2.1 with lattice vectors $\mathbf{a_1}$ and $\mathbf{a_2}$.

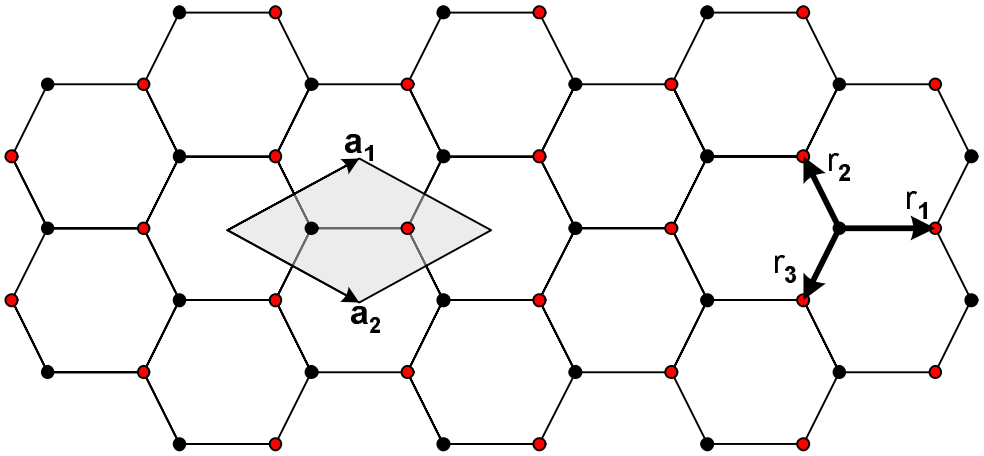

Figure 2.1: Unit cell for graphene containing two carbon atoms (shaded region). Adapted from [18]. *Black indicates atom #1 and red atom #2.*

The electron configuration of carbon in the ground state is as follows:

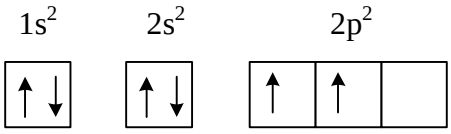

where the $1s^2$ orbital contains the core (or tightly bound) electrons and the $2s^2$ and $2p^2$ orbitals consist of four valance electrons that form the covalent bonds between the carbon

atoms. These atomic orbitals provide basis functions enabling us to establish the Hamiltonian for graphene (as reported in [19]). In graphene and carbon nanotubes there are three strong σ bonds formed by sp^2 hybridization between a 2s orbital and two 2p orbitals ($2p_x$ and $2p_y$) and one weaker π bond existing within the $2p_z$ orbital [20]. It is these π electrons that dominate the transport properties in carbon nanotubes because they form a continuous energy band near the Fermi energy, whereas the σ states have an energy gap [21]. Thus, when considering the number of basis functions or Bloch states we will require per unit cell, we only consider the $2p_z$ orbitals, consequently there are two Bloch wave functions per unit cell since there are two atoms. A depiction of the atomic orbitals and hybrid orbitals of carbon is shown in Figure 2.2.

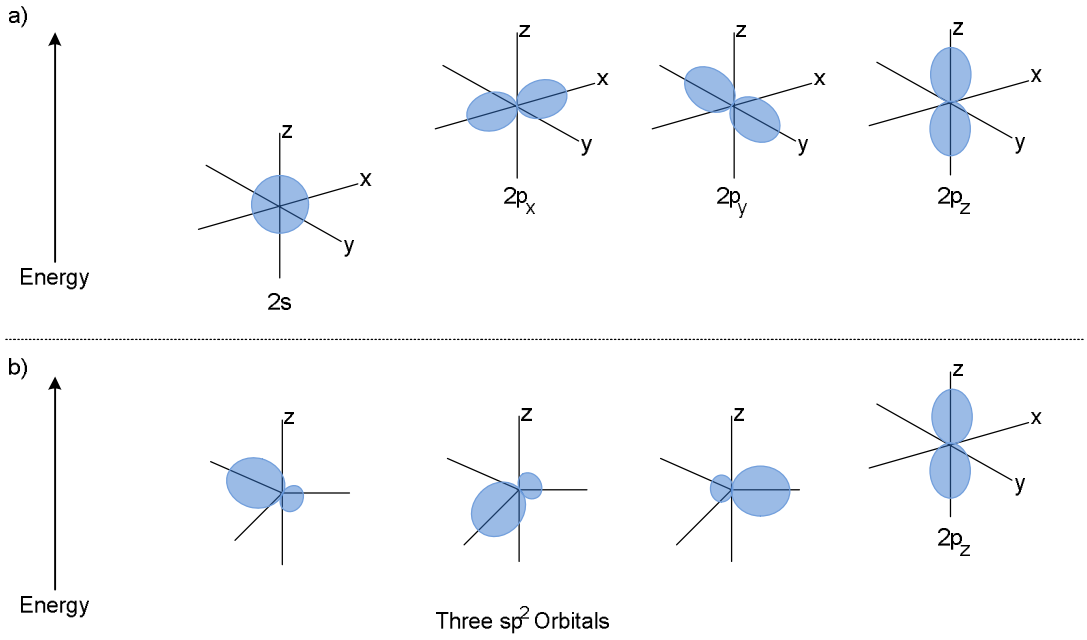

Figure 2.2: a) Atomic orbitals and b) hybrid orbitals of carbon. Adapted from [22].

The Hamiltonian Operator

The eigenvalues of the Hamiltonian operator given by the nearest neighbor tight binding approximation for graphene are calculated using equation (2.2) as reported by [23].

$$E(\vec{k}) = E_o \pm \left| \sum_{i=1}^{3} t \exp(-j\vec{k} \cdot r_i) \right| \tag{2.2}$$

In graphene, the summation is over i=1 to i=3 because there are three carbon atoms near a single atom (i.e. three nearest neighbors) as shown by the vectors $\vec{r}$ drawn in Figure 2.1. E_o is the energy of the p_z orbital and t is the hopping integral or transfer integral representing the tight binding overlap energy between a C-C bond, which has a value approximately equal to -2.72 eV [20, 21]. In order to understand where (2.2) comes from we will begin with the transfer integral matrix for the tight binding approximation of graphene given in (2.3), where n is the number of atomic orbitals per unit cell (in our case n = 2) from the π orbital of each of the two atoms.

$$H_{jj'}(\vec{k}) = \left\langle \psi_j \middle| H \middle| \psi_{j'} \right\rangle \qquad j, j' = 1,2,...,n \tag{2.3}$$

The Hamiltonian can be represented as an n x n matrix, with off diagonal elements representing the contribution from a single atom and its three nearest neighbors as indicated by the vectors **r_1, r_2, and r_3** in Figure 2.1. The value of the elements on the diagonal are equal to the energy of the p_z orbital, which is taken as a reference and set equal to zero [20]. Thus, the matrix Hamiltonian will have the form (2.4), where the subscripts 1 and 2 indicate atom #1 and atom #2 from Figure 2.1.

$$H = \begin{pmatrix} H_{11} & H_{12} \\ H_{21} & H_{22} \end{pmatrix} \tag{2.4}$$

The expression for H_{12} is given by (2.4) and $H_{12} = H_{21}^*$ because the Hamiltonian is a Hermitian matrix [20].

$$H_{12} = t(e^{j\vec{k}r_1} + e^{j\vec{k}r_2} + e^{j\vec{k}r_3}) = tf(k) \tag{2.5}$$

Now, let's break the vectors in the exponent into x and y components and determine f(k) using the following steps (Note: the lattice constant $a = \sqrt{3}a_{c-c}$ where $a_{c\text{-}c}$ is the bond length):

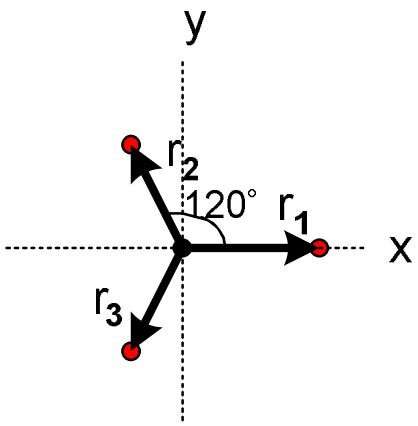

Figure 2.3: Diagram of vectors between atom #1 and the three neighboring atoms [20].

Step 1: Separate vectors into x and y components.

$$\vec{k}\,r_1 = \frac{a}{\sqrt{3}}\vec{k}_x \qquad \vec{k}\,r_2 = -\frac{a}{2\sqrt{3}}\vec{k}_x + \frac{a}{2}\vec{k}_y$$

$$\vec{k}\,r_3 = -\frac{a}{2\sqrt{3}}\vec{k}_x - \frac{a}{2}\vec{k}_y \tag{2.6}$$

Step 2: Plug (2.6) into (2.5) and determine expression for elements of the Hamiltonian.

$$H_{12} = t\left\{\exp\left(j\frac{a}{\sqrt{3}}\vec{k}_x\right) + \exp\left(-j\frac{a}{2\sqrt{3}}\vec{k}_x + j\frac{a}{2}\vec{k}_y\right) + \exp\left(-j\frac{a}{2\sqrt{3}}\vec{k}_x - j\frac{a}{2}\vec{k}_y\right)\right\}$$

$$= t\left\{\exp\left(j\frac{a}{\sqrt{3}}\vec{k}_x\right) + \exp\left(-j\frac{a}{2\sqrt{3}}\vec{k}_x\right)\exp\left(j\frac{a}{2}\vec{k}_y\right) + \exp\left(-j\frac{a}{2\sqrt{3}}\vec{k}_x\right)\exp\left(-j\frac{a}{2}\vec{k}_y\right)\right\}$$

$$= t\left\{\exp\left(j\frac{a}{\sqrt{3}}\vec{k}_x\right) + \exp\left(-j\frac{a}{2\sqrt{3}}\vec{k}_x\right)\left[\exp\left(j\frac{a}{2}\vec{k}_y\right) + \exp\left(-j\frac{a}{2}\vec{k}_y\right)\right]\right\}$$

$$= t\left\{\exp\left(j\frac{a}{\sqrt{3}}\vec{k}_x\right) + 2\exp\left(-j\frac{a}{2\sqrt{3}}\vec{k}_x\right)\cos\left(\frac{a}{2}\vec{k}_y\right)\right\} = tf(k) \tag{2.7}$$

$$H = \begin{pmatrix} 0 & tf(k) \\ tf(k)^* & 0 \end{pmatrix} \tag{2.8}$$

Step 3: Determine the eigenvalues from (2.8) which can be simplified into the form shown in (2.10) that is reported by [20].

$$\left|\begin{pmatrix} 0-E & tf(k) \\ tf(k)^* & 0-E \end{pmatrix}\right| = E^2 - t^2\left|f(k)\right|^2 = 0 \tag{2.9}$$

$$E(k) = \pm t\sqrt{|f(k)|^2} = \pm t\sqrt{1 + 4\cos\left(\frac{ak_y}{2}\right)\cos\left(\frac{\sqrt{3}ak_x}{2}\right) + 4\cos^2\left(\frac{ak_y}{2}\right)} \qquad (2.10)$$

We have successfully found the expression for the eigenvalues of the Hamiltonian for graphene which can be used to plot the energy dispersion relations depicted in Figure 2.4.

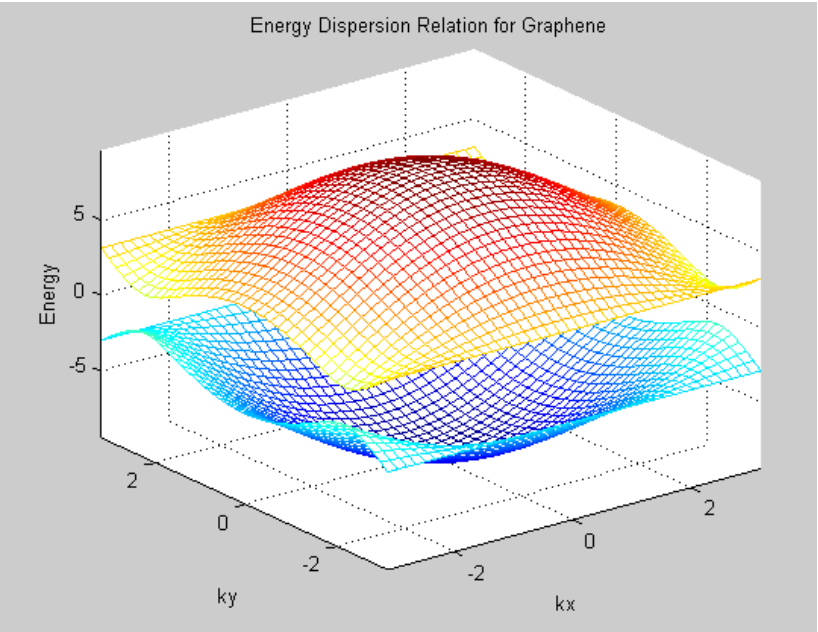

Figure 2.4: Energy dispersion relation for graphene.

We can determine the energy dispersion relation for carbon nanotubes by using our expression for graphene (2.10) and recognizing that there is a new boundary condition imposed after rolling the graphene sheet into a cylinder. Recall from Chapter 1 the circumferential vector

$$\vec{C} = n\vec{a}_1 + m\vec{a}_2 = (n, m). \qquad (2.11)$$

Substituting $\vec{a}_1$ and $\vec{a}_2$ into (2.11) gives us (2.13):

$$\vec{a}_1 = \hat{x}\frac{\sqrt{3}}{2}a + \hat{y}\frac{a}{2} \qquad \vec{a}_2 = \hat{x}\frac{\sqrt{3}}{2}a - \hat{y}\frac{a}{2} \tag{2.12}$$

$$\vec{C} = \hat{x}\frac{\sqrt{3}}{2}a(n+m) + \hat{y}\frac{a}{2}(n-m). \tag{2.13}$$

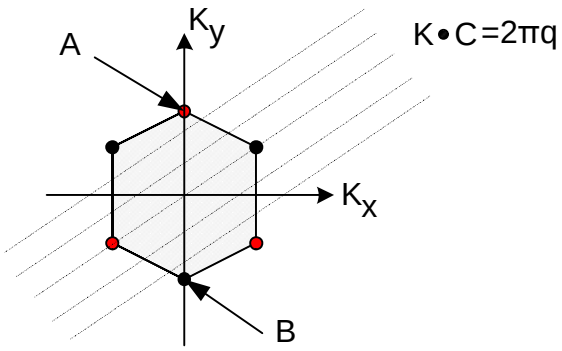

Figure 2.5: Reciprocal lattice of graphite including straight lines $K \cdot C = 2\pi q$ which indicate the new boundary conditions imposed after connecting each end of a single line together and rolling into CNT. Adapted from [19].

The new periodic boundary condition introduced after rolling the graphene sheet into a CNT by connecting the parallel lines drawn for every integer value q shown in Figure 2.5 is given by (2.14) [19].

$$\vec{k} \cdot \vec{C} = k_c|C| = k_x\frac{\sqrt{3}}{2}a(n+m) + k_y\frac{a}{2}(n-m) = 2\pi q \tag{2.14}$$

Using (2.10) and (2.14) together we are able to determine a set of energies for each value of q. The CNT will be metallic if there is no band gap present between these sets near

E=0, which occurs when one of the lines formed from equation (2.14) pass through either point A or B on Figure 2.5. These points correspond to the following:

$$A \rightarrow \left(\frac{\sqrt{3}a}{2} k_x, \frac{a}{2} k_y \right) = \left(0, \frac{2\pi}{3} \right) \tag{2.15}$$

$$B \rightarrow \left(\frac{\sqrt{3}a}{2} k_x, \frac{a}{2} k_y \right) = \left(0, -\frac{2\pi}{3} \right) \tag{2.16}$$

From (2.15) and (2.16) we can obtain (1.6), which told us whether the CNT would be metallic or semiconducting based upon the chiral coefficients n and m. For example, if a line were to pass through point A the following must be true:

$k_x = 0$ and $\frac{a}{2} k_y = \frac{2\pi}{3}$ giving us $\vec{k} \cdot \vec{C} = 0 \cdot (n+m) + \frac{2\pi}{3}(n-m) = 2\pi q \Rightarrow \frac{n-m}{3} = q$.

Therefore, a CNT will be semiconducting for all cases except when $|n-m|$ is a multiple of three because n, m, and q are integers.

Energy Dispersion Relation for Zigzag CNTs

As discussed in Chapter 1, carbon nanotubes can either be zigzag, armchair, or chiral depending upon the coefficients n and m. In order to have a zigzag tube m=0 so that $\vec{C} = (n,0)$, meaning that the circumferential vector has a magnitude $|\vec{C}| = a \cdot n$ with the periodic boundary condition requiring that the k values are perpendicular to the k_y axis lying completely in the $\vec{k}_x$ direction as depicted in Figure 2.6. Therefore, (2.14) gives us the following constraint on the possible k_y values:

$$ank_y = 2\pi q \Rightarrow k_y = \frac{2\pi q}{an} \qquad \text{with } q = 1,2,3...,2n. \tag{2.17}$$

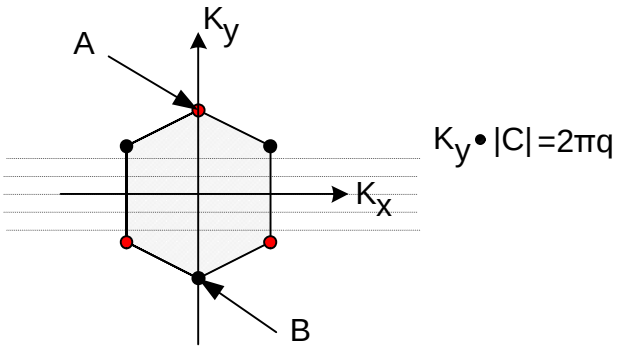

Figure 2.6: Reciprocal lattice of graphite including straight lines $K_y \cdot |C| = 2\pi q$ resulting in a zigzag carbon nanotube. Adapted from [19].

After applying (2.17) to (2.10) we obtain the energy dispersion relation for zigzag carbon nanotubes (2.18).

$$E(k) = \pm t\sqrt{|f(k)|^2} = \pm t\sqrt{1 \pm 4\cos\left(\frac{q\pi}{n}\right)\cos\left(\frac{\sqrt{3}ka}{2}\right) + 4\cos^2\left(\frac{q\pi}{n}\right)} \tag{2.18}$$

$$for\ -\frac{\pi}{\sqrt{3}} < ka < \frac{\pi}{\sqrt{3}} \quad and \quad q = 1,2,3,...,2n$$

Two different examples implementing equation (2.18) are shown in Figures 2.7 and 2.8 representing a semiconducting and metallic CNT respectively.

(a)

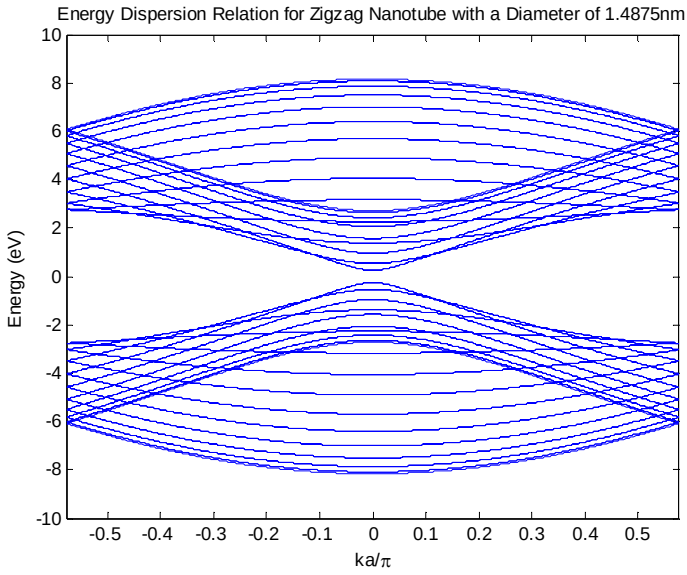

(b)

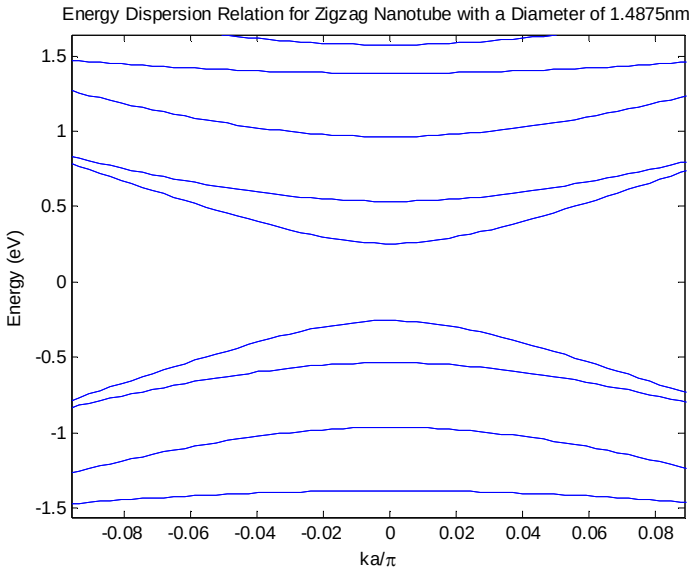

Figure 2.7: Energy dispersion relation for a semiconducting zigzag nanotube with a diameter of ~1.49nm (a) shows all possible energy bands (b) energy bands near the Fermi level (t=-2.72eV, n=19, m=0, E_o=0).

(a)

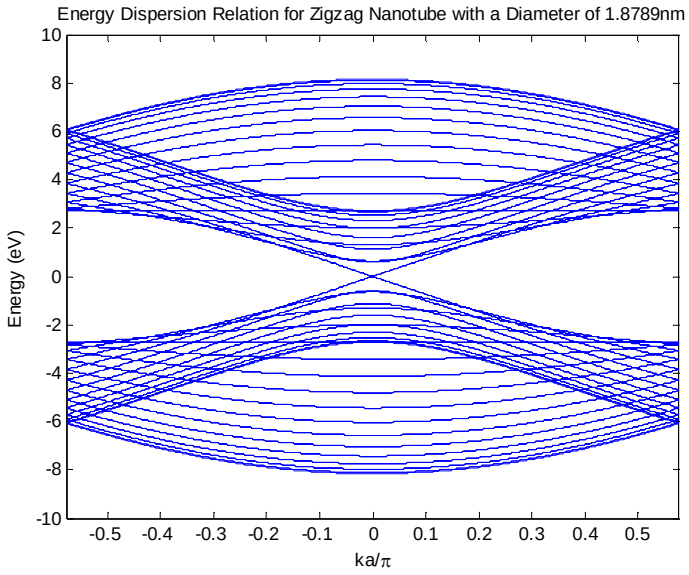

(b)

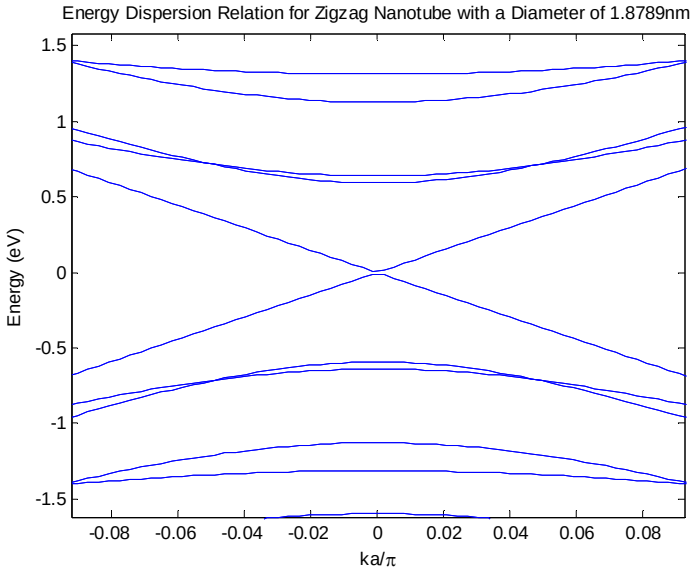

Figure 2.8: Energy dispersion relation for a metallic zigzag nanotube with a diameter of ~1.88nm (a) shows all possible energy bands (b) energy bands near the Fermi level (t=-2.72eV, n=24, m=0, E_o=0).

There are a total of four channels (two arising from the band structure in relation to the C-C bonds themselves and an additional two from taking into account spin). Thus CNTs should have a maximum conductance equal to ~$4G_o$ when assuming there is no scattering i.e. ballistic transport [18]. G_o is a fundamental constant equal to $\frac{e^2}{h}$ representing the maximum allowed conductance per channel of a 1-D conductor (later in this chapter we will derive G_o). To date, it has been demonstrated that metallic CNTs come very close to achieving the maximum conductance value, while semiconducting tubes have been able to attain values up to 25% of G_o at room temperature [24]. The primary reason 100% G_o has not been achieved is due to imperfect contacts.

Energy Dispersion Relation for Armchair CNTs

The same approach used in the previous section can be applied to armchair CNTs which have the property n=m (i.e. $\vec{C} = (n, n)$). This time, however, the allowed values of k will be perpendicular to the k_x axis as shown in Figure 2.9 with the boundary condition defined by (2.19) and the magnitude of the circumferential vector still $\left|\vec{C}\right| = a \cdot n$. Notice that all armchair CNTs will be metallic because at least one of the subbands will always pass through point A and B as indicated in Figure 2.9 independent of the value of n [19].

$$\sqrt{3}ank_x = 2\pi q \Rightarrow k_x = \frac{2\pi q}{\sqrt{3}an} \qquad \text{with } q = 1,2,3...,2n \tag{2.19}$$

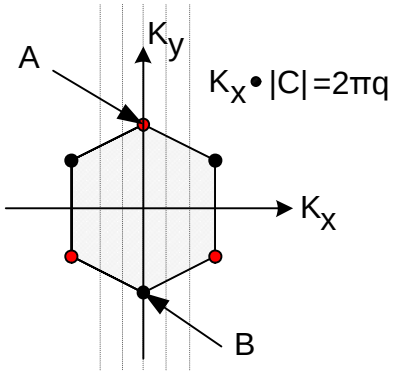

Figure 2.9: Reciprocal lattice of graphite including straight lines $K_x \cdot |C| = 2\pi q$ resulting in an armchair carbon nanotube. Adapted from [19].

Applying the condition from (2.19) into (2.10) results in the following energy eigenvalues:

$$E(k) = \pm t\sqrt{|f(k)|^2} = \pm t\sqrt{1 \pm 4\cos\left(\frac{q\pi}{n}\right)\cos\left(\frac{ka}{2}\right) + 4\cos^2\left(\frac{ka}{2}\right)} \qquad (2.20)$$

$$for\ -\pi < ka < \pi \qquad and \qquad q = 1,2,3,\ldots,2n$$

As before, Figure 2.10 contains a plot as an example of the energy dispersion relation given in (2.20).

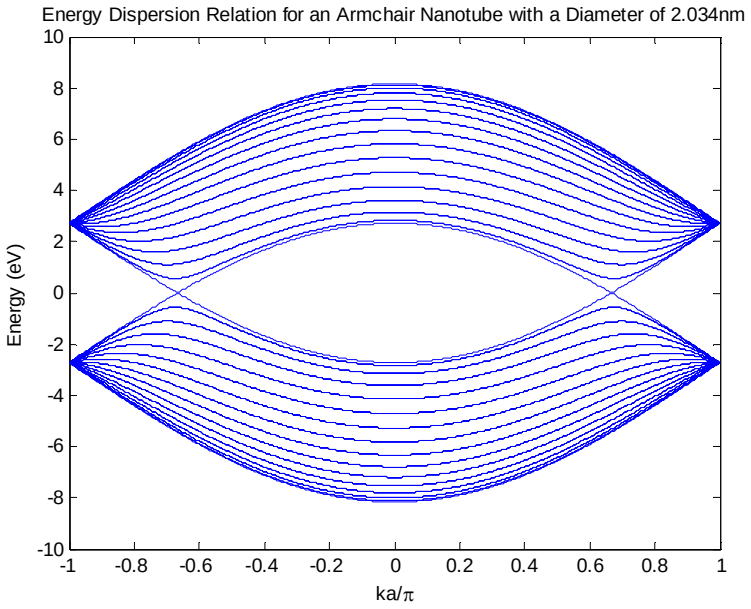

Figure 2.10: Energy dispersion relation for a metallic armchair nanotube with a diameter of ~2.034nm (t=-2.72eV, m=n=15, E_o=0).

Size of the Energy Band Gap in Semiconducting CNTs

In Chapter 1 we discussed the inverse relationship of the size of the band gap $E_g \approx \frac{1}{d}$, where d is the diameter of the tube. This approximation can be derived mathematically using some of our results discussed in the previous two sections. Due to the fact that the electrical conduction in a carbon nanotube comes from the available states near the Fermi energy it is possible to calculate an approximation to the area close to the Fermi level (E=0 of Figures 2.8 and 2.10) that sufficiently describes the electrical conduction [19]. This approximation will be a simplification of equation (2.18) for the zigzag CNT from a Taylor expansion around the points described in (2.15) and (2.16) where E=0. The simplified equation can be used to illustrate how to determine an

expression for the energy band gap of a CNT.

Let us begin by returning to equation (2.10) where f(k) can be written as

$$f(k) = -t\left(1 + 2\exp\left[\frac{j\sqrt{3}ak_x}{2}\right]\cos\left(\frac{ak_y}{2}\right)\right) \tag{2.21}$$

which is an "easier" equation for calculating a Taylor expansion around E=0. Recall that the points we are expanding around are $\frac{\sqrt{3}}{2}ak_x = 0$ and $\frac{ak_y}{2} = \pm\frac{2\pi}{3}$ and as expected the first term of the expansion will be zero. The second term yields the following as reported by [19]:

$$f(k) \approx k_x\left|\frac{\partial f(k)}{\partial k_x}\right|_{\frac{\sqrt{3}}{2}k_x a=0,\frac{ak_y}{2}=\pm\frac{2\pi}{3}} + \left(k_y \mp \frac{4\pi}{3a}\right)\left|\frac{\partial f(k)}{\partial k_y}\right|_{\frac{\sqrt{3}}{2}k_x a=0,\frac{ak_y}{2}=\pm\frac{2\pi}{3}} \tag{2.22}$$

Below is the calculation of the partial derivatives in (2.22)

$$\left|\frac{\partial f(k)}{\partial k_x}\right|_{\frac{\sqrt{3}}{2}k_x a=0,\frac{ak_y}{2}=\pm\frac{2\pi}{3}} = -tj\sqrt{3}a\left(-\frac{1}{2}\right) = jt\frac{\sqrt{3}}{2}a \tag{2.23}$$

$$\left|\frac{\partial f(k)}{\partial k_y}\right|_{\frac{\sqrt{3}}{2}k_x a=0,\frac{ak_y}{2}=\pm\frac{2\pi}{3}} = at\sin\left(\pm\frac{2\pi}{3}\right) = \pm\frac{\sqrt{3}}{2}at \tag{2.24}$$

which yields

$$f(k) \approx \frac{\sqrt{3}}{2}at\left[jk_x \pm \left(k_y \mp \frac{4\pi}{3a}\right)\right] \tag{2.25}$$

and

$$E(k) = \pm\left|f(k)\right| = \pm\frac{\sqrt{3}}{2}at\sqrt{k_x^2 + \left(k_y \mp \frac{4\pi}{3a}\right)^2}\,. \tag{2.26}$$

Now we will choose to write the energy dispersion relation for a zigzag nanotube by incorporating equations (2.17) and (2.26) from which we can estimate the energy gap.

$$E(k_x)_{zigzag} = \pm\frac{\sqrt{3}}{2}at\sqrt{k_x{}^2 + \left[\frac{4\pi}{3a}\left(\frac{3q}{2n} - 1\right)\right]^2} \tag{2.27}$$

The bandgap for subband q is equal to the difference between the positive and negative values of $E(k_x)$ at k_x=0 [19].

$$E_{gap,q} = 2E(k_x)_{zigzag} = \sqrt{3}at\frac{4\pi}{3a}\left(\frac{3q}{2n} - 1\right) = \frac{6\pi a_{c-c}t}{an}\left(q - \frac{2n}{3}\right) \tag{2.28}$$

The minimum value of $\left(q - \frac{2n}{3}\right)$ when n is not a multiple of 3 (i.e. CNT is semiconducting) is equal to 1/3 [19]. Thus the minimum possible energy band gap is equal to (2.29) where we include the fact that the circumference $C = \pi d = an$ with d being the diameter.

$$E_{gap} = \frac{2\pi a_{c-c}t}{an} = \frac{2a_{c-c}t}{d} \approx \frac{0.8eV}{d} \tag{2.29}$$

This approximation confirms the inverse proportionality of the band gap to the diameter discussed earlier in chapter 1.

Kronig-Penney Model

The previous section described how an approximation to the band structure could be accomplished through the use of the tight binding model. This also allowed us to mathematically verify the estimation of the energy band gap present in semiconducting SWCNTs reported in Chapter 1. Now an approximation of the energy dispersion relation will be calculated using the Kronig-Penney model. Although slightly different, this model involves many of the same concepts we used earlier, mainly that the periodicity of the two atoms within the unit cell give rise to a periodic potential as illustrated in Figure 2.11.

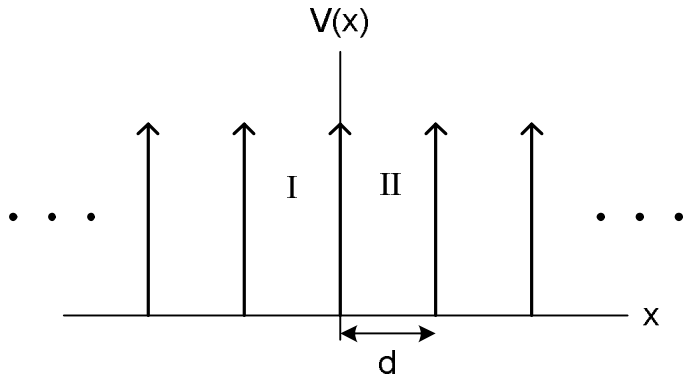

Figure 2.11: Periodic potential where d is the lattice separation length.

$$V(x) = \sum_{n=-\infty}^{\infty} V_o \delta(x - nd) \tag{2.30}$$

$$V(x) = V(x + d) \tag{2.31}$$

The Hamiltonian of the system described in Figure 2.11 is

$$H = \frac{P_{op}^{\ 2}}{2m} + V(x) \tag{2.32}$$

and the wave function (or Bloch state) for regions II and I are (2.33) and (2.34) respectively.

$$\Psi_{II}(x) = Ae^{ikx} + Be^{-ikx} \text{ with } k = \sqrt{\frac{2mE}{\hbar^2}} \tag{2.33}$$

$$\Psi_{II}(x+d) = e^{iqd}\Psi_I(x) \Rightarrow \Psi_I(x) = e^{-iqd}\psi_{II}(x+d) = e^{-iqd}\left[Ae^{ik(x+d)} + Be^{-ik(x+d)}\right]$$

$$\Psi_I(x) = e^{-iqd}\left[Ae^{ik(x+d)} + Be^{-ik(x+d)}\right] \tag{2.34}$$

We will now apply the boundary conditions recognizing that the wave function must be continuous at x=0.

<u>At x=0:</u>

$$\Psi_{II}(0) = A + B \qquad \text{and} \qquad \Psi_I(0) = e^{-iqd}\left[Ae^{ikd} + Be^{-ikd}\right] \tag{2.35}$$

The first derivative of the wave function is discontinuous thus we must employ the following condition:

$$\lim_{\varepsilon \to 0}\left[\Psi_{II}'(\varepsilon) - \Psi_I'(-\varepsilon)\right] = \frac{2mV_o}{\hbar^2}\Psi(0) \tag{2.36}$$

The boundary conditions are (2.36) and (2.37) which provide a set of two equations that must be solved in order to provide the solution to the relationship between the energy (E) and qd similar to what was calculated for the tight binding approximation.

$$\Psi_I(0) = \Psi_{II}(0) \tag{2.37}$$

After applying (2.36) and (2.37) we get the following two equations:

$$A + B = e^{-iqd}\left[Ae^{ikd} + Be^{-ikd}\right] \tag{2.38}$$

and $$V_o(A+B) = i\frac{\hbar^2 k}{2m}\left[A - B - e^{-iqd}\left(Ae^{ikd} - Be^{-ikd}\right)\right] \tag{2.39}$$

which when combined yield the following condition:

$$\cos(qd) = \cos(kd) + \frac{mV_o d}{\hbar^2}\left(\frac{\sin(kd)}{kd}\right) \tag{2.40}$$

A plot of the energy dispersion relation (or E versus qd spanning $-\pi \le qd \le \pi$) is shown in Figure 2.12, where d=2.46 Å. This plot was made solving equation (2.40), where we only need to input the effective mass of the particle and shape or width of the periodic potential. The effective mass can be calculated by (2.41) and (2.42) for chiral and zigzag/armchair tubes respectively as reported in [25]. For simplicity we will consider a zigzag CNT with a diameter of 1.5nm which yields $m^* = 0.06311 m_e$.

$$m^*(D_{CNT})_{chiral} = \frac{29}{2} m_e \left(\frac{a_{c-c}}{D_{CNT}}\right)^{\left[\frac{\pi}{2} + \frac{26\pi}{7}\left(\frac{a_{c-c}}{D_{CNT}}\right) - \frac{37\pi}{3}\left(\frac{a_{c-c}}{D_{CNT}}\right)^2\right]} \tag{2.41}$$

$$m^*(D_{CNT})_{zigzag/armchair} = \frac{2}{3} m_e \left(\frac{a_{c-c}}{D_{CNT}}\right) \tag{2.42}$$

As expected this gives a similar result as calculated in the previous section.

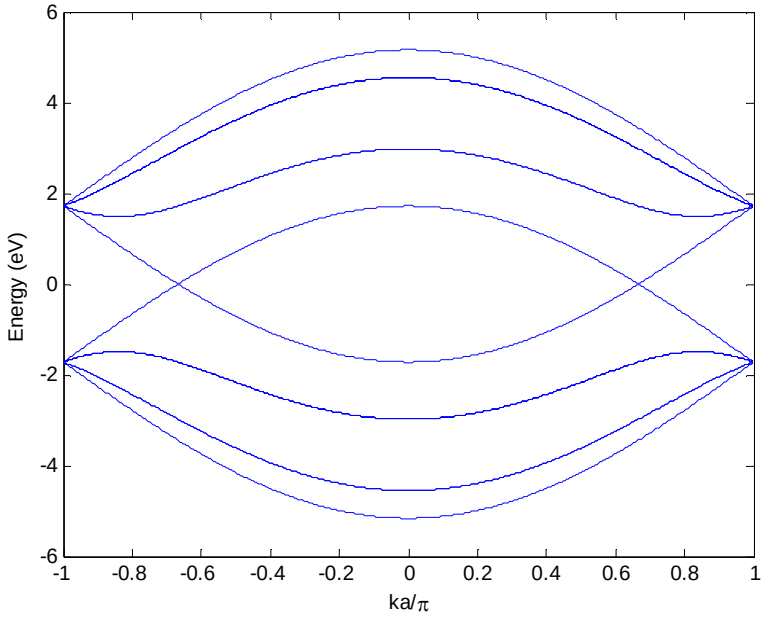

Figure 2.12: Energy Dispersion Relation using Kronig Penney Model

Conductance in 1-D Systems and CNTs

Conductance in 1-D systems and Carbon Nanotubes

If we consider the case of ballistic transport or approach the conductance of a wire with infinitesimal length so that there is no increase in resistance due to scattering, there is a fundamental constant for 1-D systems that describes the maximum achievable conductance. This constant is given by

$$G_o = q^2 / h = \frac{1}{25.8k\Omega} \tag{2.43}$$

In actuality, this value will be twice as much because 1-D systems have at least two channels, one for up spin and one for down spin of the electron [19]. Carbon nanotubes

have a total of four channels, therefore, the maximum possible conductance for one tube (assuming perfect contacts) will be four times as much as the fundamental constant, G_o. This means that the lowest possible series resistance of a CNT with ideal contacts is ~6.45 kΩ irrespective of length, which is still high if we want to build an effective matching network at high frequencies. However, the contacts to CNTs are generally nowhere near ideal. The contact resistance dominates to such an extent that the total series resistance can be on the order of 40-50 times larger than 6.45 kΩ, which poses even greater difficulties. The detrimental contact resistance can be mitigated somewhat by aligning several nanotubes in parallel across the electrodes.

Derivation of the Fundamental Constant G_o

For more completeness it may be useful to understand the origins for the fundamental constant G_o which indicates the presence of a limit to the maximum current that can flow through a device. Let us begin by thinking of a single one-level device in which a voltage is applied across the source and drain as depicted in Figure 2.13 and where the energy level ε is between the electrochemical potentials μ_1 and μ_2. The current through the channel is equal to (2.44). (The development of G_o is accomplished by utilizing information in [19]).

$$I = \frac{q}{\hbar}\frac{\gamma_1\gamma_2}{\gamma_1+\gamma_2} \tag{2.44}$$

In equation (2.44) γ_1 and γ_2 are related to the coupling to the contacts ($\gamma/\hbar$ is equal to the rate at which an electron at energy ε will escape and transfer into the contacts). For

simplicity we can assume that the coupling to the source and drain are equal ($\gamma = \gamma_1 = \gamma_2$). Thus,

$$I = \frac{q\gamma}{2\hbar}. \tag{2.45}$$

The above equation for the current ignores the fact that the energy level between μ_1 and μ_2 will broaden beyond the area between μ_1 and μ_2 where current flows [19]. Thus, the current described by (2.45) will decrease in value by a factor proportional to $\frac{\mu_1 - \mu_2}{A\gamma}$ that corresponds to the fraction of the energy level that is within $\mu_1 \leq E \leq \mu_2$ with γA being a constant related to the effective width of the energy level. After taking the above into account along with the fact that $qV_D = \mu_1 - \mu_2$ the actual current through the channel will be

$$I = \frac{q\gamma}{2\hbar}\frac{qV_D}{A\gamma} = \frac{q^2V_D}{2\hbar A} \tag{2.46}$$

and the conductance

$$G = \frac{I}{V_D} = \frac{q^2}{2\hbar A}. \tag{2.47}$$

An other way of looking at this is that the coupling to the contact results in the spreading of a single energy level into a continuous density of states around the single energy level as shown in Figure 2.13 (b). The broadening $\beta = \gamma_1 + \gamma_2$, indicates that the more we

couple to the contacts the larger the broadening of the energy level. The density of states consequent to the spread of the energy level can be described as

$$D(E) = \frac{\beta/2\pi}{(E-\varepsilon)^2 + (\beta/2)^2} \tag{2.48}$$

and the current between the contacts can be calculated using equation (2.49) [19].

$$I = \frac{q}{\hbar}\frac{\gamma_1\gamma_2}{\gamma_1+\gamma_2}\int_{\mu_2}^{\mu_1} D(E)dE \tag{2.49}$$

Equation (2.49) becomes

$$I = \frac{q}{\hbar}\frac{\gamma_1\gamma_2}{\gamma_1+\gamma_2} D * (\mu_1 - \mu_2) \tag{2.50}$$

and if we assume that the density of states is constant between $\mu_2 \leq E \leq \mu_1$ then

$$I = \frac{q}{\hbar}\frac{\gamma_1\gamma_2}{\gamma_1+\gamma_2}(\mu_1-\mu_2)\frac{\beta/2\pi}{(E-\varepsilon)^2+(\beta/2)^2} = \frac{q}{\hbar}\frac{\gamma_1\gamma_2}{\gamma_1+\gamma_2}(\mu_1-\mu_2)\frac{(\gamma_1+\gamma_2)/2\pi}{\left(\frac{\mu_1+\mu_2}{2}-\varepsilon\right)^2+((\gamma_1+\gamma_2)/2)^2}$$

$$= \frac{q}{\hbar}\frac{\gamma_1\gamma_2}{\gamma_1+\gamma_2}(\mu_1-\mu_2)\frac{(\gamma_1+\gamma_2)/2\pi}{(\mu-\varepsilon)^2+((\gamma_1+\gamma_2)/2)^2} \tag{2.51}$$

The maximum current occurs when the energy level is equal to μ. Therefore, the maximum current is equal to

$$I_{\max} = \frac{q}{h}\frac{4\gamma_1\gamma_2(\mu_1-\mu_2)}{(\gamma_1+\gamma_2)^2} = \frac{q}{h}\frac{4\gamma_1\gamma_2(qV_D)}{(\gamma_1+\gamma_2)^2} = \frac{q^2}{h}\frac{4\gamma_1\gamma_2}{(\gamma_1+\gamma_2)^2}V_D \tag{2.52}$$

and the maximum conductance

$$G = \frac{I}{V_D} = \frac{q^2}{h}\frac{4\gamma_1\gamma_2}{(\gamma_1+\gamma_2)^2} = \frac{q^2}{h}\frac{4\gamma^2}{(2\gamma)^2} = \frac{q^2}{h} = G_o \tag{2.53}$$

when $\gamma = \gamma_1 = \gamma_2$.

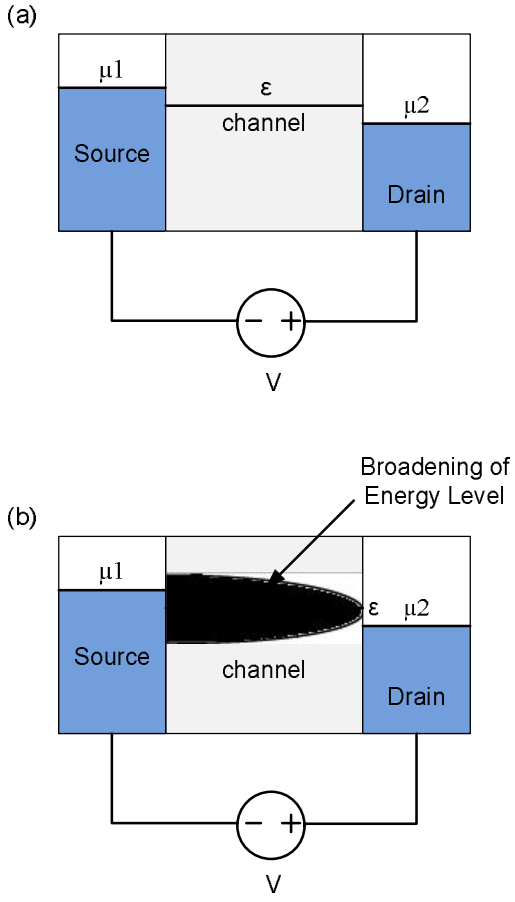

Figure 2.13: (a) Voltage applied across a channel leading to a splitting of the source and drain electrochemical potentials μ_1 and μ_2, where ε represents the energy level. (b) Representation of the presence of broadening of the energy level due to coupling to the channel which causes part of the energy level to go beyond the energy between μ_1 and μ_2 [19].

Ballistic Transport

Due to their pure structure the transport in CNTs is ballistic, meaning that the resistance through the CNT does not increase due to the effects of scattering caused by the presence of impurities. Experimentally ballistic transport has been observed with CNTs as long as 1μm. Typically current decreases with respect to the length the electrons travel according to $\sim\frac{\mu}{L}$, but in the case of ballistic transport with the absence of scattering, the length does not influence the amount of current that travels through it. Recall that it has been proven by [17] that in fact the transport through CNTs can be ballistic, because they observed identical current values through two different channel lengths along a single tube.

Quantum Capacitance, Electrostatic Capacitance,
Magnetic and Kinetic Inductance

In 1-D systems such as CNT-based devices, the resistance can be extremely high. The capacitance, on the other hand, is usually very low, therefore, the transient times are short and the operational speed of such devices can be fast [11]. In order to fully understand the applicability of CNTs for high frequency nanoelectronics it is necessary that we determine the values for the quantum capacitance, electrostatic capacitance, magnetic and kinetic inductance present in CNTs. Since nanotubes are 1-dimensional devices, we can use the Lüttinger model to take into account the quantum effects associated with interacting electrons in 1-D systems; realizing that the overall impedance will have both a quantum capacitance and kinetic inductance component. Using the

model reported by [26] the quantum capacitance C_Q can be obtained using following equation:

$$C_Q = \frac{e^2}{\hbar \pi v_F} \tag{2.54}$$

and the electrostatic capacitance by

$$C_E = 2\pi\varepsilon / \ln(h/d), \tag{2.55}$$

where v_F is the Fermi velocity, ε the dielectric constant, d the diameter of the wire (CNT), and h the distance from the ground plane to the CNT. The total capacitance will be the series combination of these two capacitances:

$$C = \frac{C_E C_Q}{C_E + C_Q}. \tag{2.56}$$

Estimated values for the quantum and electrostatic capacitance of nanotubes are C_Q~100 aF/μm and C_E~50 aF/μm. Notice that these estimates are a function of length.

The total inductance of a single CNT is a series combination of both kinetic and magnetic inductance. The kinetic inductance for 1-Dimensional systems can be calculated by

$$L_K = \frac{\hbar \pi}{e^2 v_F}. \tag{2.57}$$

and the magnetic inductance by

$$L_M \approx \frac{\mu}{2\pi} \ln\left(\frac{h}{d}\right) \tag{2.58}$$

For carbon nanotubes these values can be approximated by the following:

$$L_K \sim 16 \text{ nH/μm} \tag{2.59}$$

$$L_M \sim 1 \text{ pH/ } \mu\text{m} \tag{2.60}$$

With these four estimates it is possible to create a circuit diagram of a nanotube as a 1-dimensional nanowire and estimate the characteristic impedance. This can be thought of as being equivalent to a transmission line with distributed capacitance and inductance per unit length. The circuit diagram in Figure 2.14 is for spinless electrons. Taking into account that the band structure of CNTs has two propagating channels and that each of these has an additional channel due to the possibility of spin up or spin down of an electron, carbon nanotubes have a total of four channels. This is incorporated into the circuit model by simply dividing the kinetic inductance by four and multiplying the quantum capacitance by four (Figure 2.15).

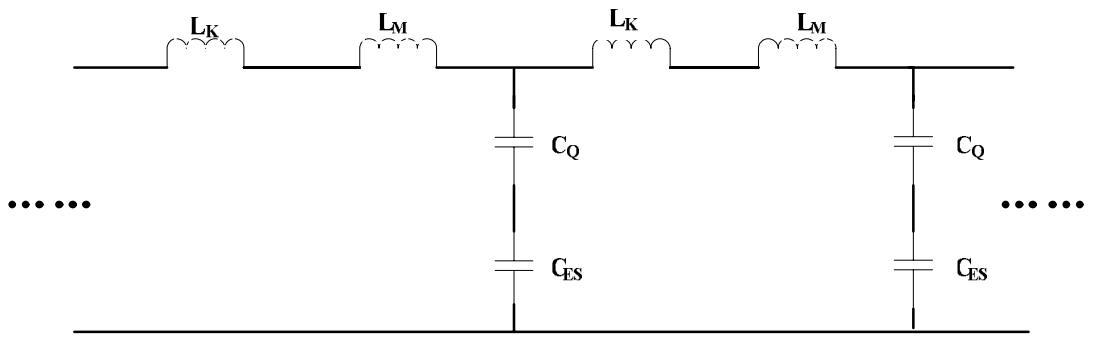

Figure 2.14: Carbon nanotube circuit model for spinless electrons [26].

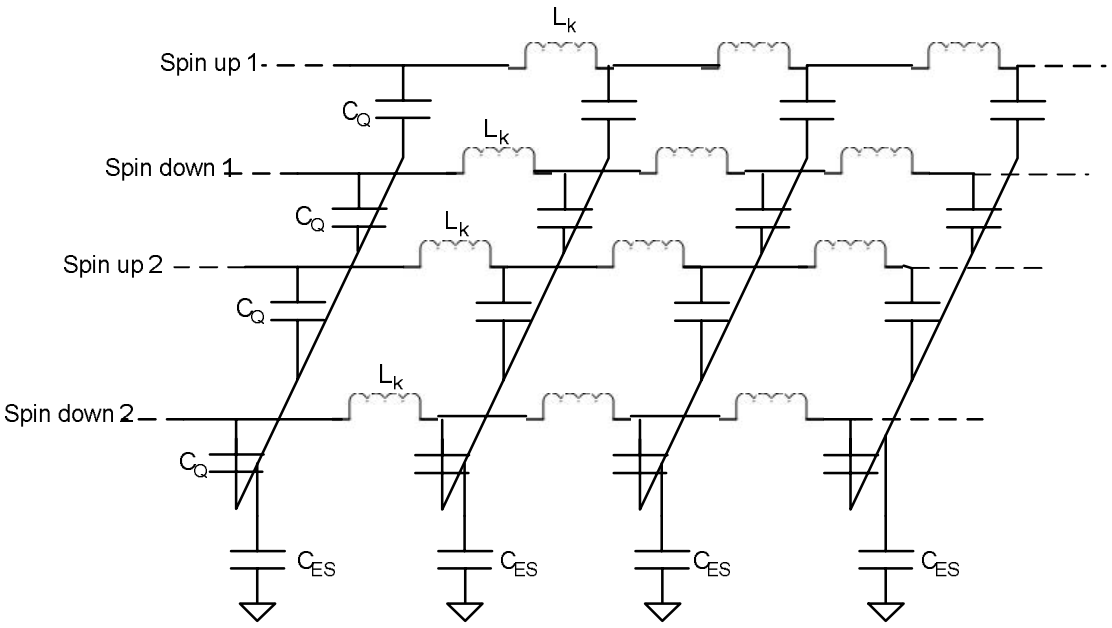

Figure 2.15: Four channel carbon nanotube circuit model for interacting electrons [26].

Summary

In the previous two chapters we developed the fundamental concepts required to understand the electronic transport in CNTs. This information is necessary for creating the CNT based Schottky diode and SBFET models discussed in the next chapter that are used for simulation purposes. In order to determine the feasibility of CNTs for high frequency applications these models will be used to simulate the operation of these devices for millimeter/submillimeter wave applications.

MODELING OF A CARBON NANOTUBE SCHOTTKY DIODE AND SCHOTTKY BARRIER FET

Overview

The goal of this chapter is to formulate an equivalent circuit for a Schottky diode realized using one or more semiconducting SWCNTs, and extrapolate the projected performance based on this model and fabrication capabilities that have been reported in the literature. We will begin by discussing a set of assumptions that are made in creating this model along with the reasoning behind why these assumptions can be valid. The final objective is to create a matching network that will match the diode to 50 Ω, determine what percentage of the input power is delivered to the load and calculate the noise equivalent power (NEP). Although theoretically we can successfully create a matching network as demonstrated by the simulations reported herein, in practice there is a significant challenge because of the large dominating series resistance caused by poor contacts and the limit on the maximum achievable conductance G_o. This leads to a very narrow bandwidth around which to operate efficiently and still have a significant percentage of the input power delivered to the load. It also necessitates the realization of nearly lossless matching networks.

The expected performance will be determined using simulated results in conjunction with the best published experimental data as of early 2009. We will consider both the ideal case (where there is no additional series resistance due to poor contacts, and the conductance of the CNT is equal to G_o) and the case where the conductance through a single CNT is equal to ~$0.25G_o$, which is representative of current capabilities

observed experimentally where the additional resistance is due to poor contacts. This chapter demonstrates that we can improve the Schottky diode by placing several CNTs in parallel. However, once we consider what has actually been achieved so far, these devices still yield significant challenges and considerable improvement must be made, particularly in the area of making contact to the tubes.

Following the discussion of the Schottky diode, there will be a brief discussion on an equivalent circuit model for a Schottky barrier FET. This section will investigate the advantages/disadvantages of placing additional tubes in parallel across the source and drain. Particularly, we will focus on the effect more parallel tubes will have on the cutoff frequency.

Diode RF Equivalent Circuit

We have already determined the capacitance and inductance of a single carbon nanotube in Chapter 2, the next step will be incorporating these into an equivalent RF circuit model. This can be done using the typical equivalent circuit for a Schottky diode [27], where the series inductance (L_p) and shunt capacitance (C_p) are equal to the total inductance and capacitance obtained from the CNT circuit model (as shown in Figure 3.1). In other words,

$$L_P = L_K + L_M \tag{3.1}$$

and

$$C_P = \frac{C_E C_Q}{C_E + C_Q} \tag{3.2}$$

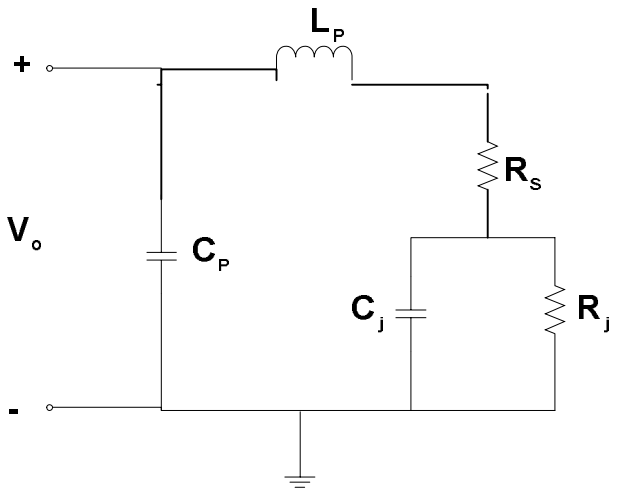

Figure 3.1: Diode RF equivalent circuit model for a Schottky diode [27].

The value of the series resistance (R_S) can be estimated by summing the resistance at the contacts and the minimum achievable resistance for a 1-D system discussed earlier.

$$R_S \approx R_{Contact} + 6.45k\Omega \tag{3.3}$$

The equivalent circuit also takes into account the junction capacitance and resistance. The junction capacitance (C_j) is dependent upon the effective contact area of the diode, therefore in our case it will be negligibly small because the nanotube area is extremely small.

$$C_j = \frac{\varepsilon_s \varepsilon_o A}{X_D} + C_o \tag{3.4}$$

$$X_D = \sqrt{\frac{2\varepsilon_s \varepsilon_o (\phi_C - V)}{qN}} \tag{3.5}$$

$$\phi_C = \phi_B - 0.026\left[1 + L_n\left(\frac{N_C}{N}\right)\right] \tag{3.6}$$

The junction capacitance can be determined by eq. (3.4)-(3.6) [28], where A is the effective contact area of the diode, ε_s the dielectric constant of the semiconductor, C_o the overlay (bonding pad) capacitance, N the doping level for the epitaxial layer, and Φ_c the contact potential. For all of the simulations reported in this thesis we will estimate $C_j \sim 0$ due to the very small area of the devices. Additionally, the junction resistance can be calculated using equation (3.9). Determining how to manipulate the value of the junction resistance will be crucial since the voltage sensitivity of the diode is directly proportional to it, thus it is desirable to achieve the maximum possible value as justified by (3.7) and (3.8). One may think that dramatically increasing R_j will have a negative impact on our ability to successfully create a matching network to the diode. However, in the case of the CNT-based device, the poor contacts and quantum conductance limit dominate the matching capabilities to the diode. Therefore, we should be able to increase the junction resistance without it strongly influencing the effectiveness of the matching network.

We have determined that there are three main factors of interest that we wish to manipulate in order to optimize performance in terms of the diode's application as an RF detector. One main factor is that the collection of parameters that are inherent to the CNT itself that can only be altered by changing the diameter and length of the nanotube (L_p and C_p) as discussed in Chapter 2. The second is to determine methods which will reduce the series resistance, consequently leading to more of the input power being delivered to the load rather than being dissipated in Rs from the model of Figure 3.1. Finally, there is the junction resistance determined by equation (3.9), which we would

like to maintain as large as possible with respect to Rs (C_j is not as important because its value will be extremely small).

The voltage sensitivity of a diode is a measure of the change in the DC output voltage in relation to the input power and the current sensitivity is a measure of the change in the DC output current with respect to the input power [27]. It is desirable to make the voltage sensitivity β_v as large as possible for detector diodes. Therefore, as shown in (3.7) and (3.8) we want to increase R_j.

$$\beta_i = \frac{\left(\frac{q}{nkT}\right)^2 (I_o + I_{Sat}) R_j}{2} \left[A/W\right] \tag{3.7}$$

$$\beta_v = \beta_i R_j \tag{3.8}$$

$$R_j = \frac{nkT}{q(I_o + I_{Sat})} \tag{3.9}$$

In the above equations I_o refers to the bias current, I_{Sat} the saturation current, and n the ideality factor of the diode which is typically between 1 and 2. How can we influence the junction resistance? From the above equation it is clear that one of the possible ways to increase R_j is to decrease the saturation current, where I_{Sat} can be calculated by

$$I_{Sat} = AA^* T^2 \exp\left[-q\phi_B/(kT)\right] \tag{3.10}$$

where A is the diode area, A^* the effective Richardson constant, and ϕ_B the barrier height at the CNT-metal junction.

$$A^* = \frac{4\pi q m^* k^2}{h^3} \tag{3.11}$$

Therefore, if we decrease the area of the diode or increase the barrier height at the CNT-metal junction we will decrease the magnitude of the saturation current and thus enlarge the junction resistance.

In summary, all of the above equations indicate that we would like to decrease R_s without simultaneously decreasing R_j. This can be achieved by placing several CNTs in parallel across the contacts as long as a few assumptions described in the next section are accurate. If these assumptions prove to be false, little to no improvement will be made when placing CNTs in parallel across the contacts. This is because both R_j and R_s will decrease simultaneously and thus power delivery to the load cannot be improved due to a significant portion of the power still being dissipated in R_s.

Assumptions Made in Creating Equivalent Circuit

The main assumption made for these simulations is that when we add CNTs in parallel we are adding an additional four channels (~6.45 kΩ in parallel) per tube and thus in effect the series resistance will decrease as Rs = 6.45 kΩ/n where n is the number of tubes in parallel (the 6.45 kΩ assumes conductance=G_o). In conjunction with this we assume that R_j does not decrease significantly and that each tube does not add an extra R_j component in parallel in our equivalent circuit. In other words, we propose that each additional CNT will be close enough to one another so that we need not treat each CNT as creating an entirely separate "diode" in parallel. This allows us to associate a single R_j component to the device, regardless of the number of tubes, that will decrease by a negligible amount because of the very small increase in the contact area associated with additional tubes. A basic depiction of the effect of adding parallel tubes to the

equivalent circuit model of Figure 3.1 is shown in Figure 3.2. The value of Z_{in} is determined by (3.12) where C_{ptotal} and L_{ptotal} is the total capacitance and inductance dependent upon the total number of tubes, n.

$$Z_{in} = \left(j\omega C_{ptotal} + \frac{1}{R_Q + R_C + j\omega L_{ptotal} + \frac{1}{\frac{1}{R_j} + j\omega C_j}} \right)^{-1} \tag{3.12}$$

$$L_{ptotal} = \frac{L_p}{n} \tag{3.13}$$

$$C_{ptotal} = nC_p \tag{3.14}$$

$$R_S = R_Q + R_C \tag{3.15}$$

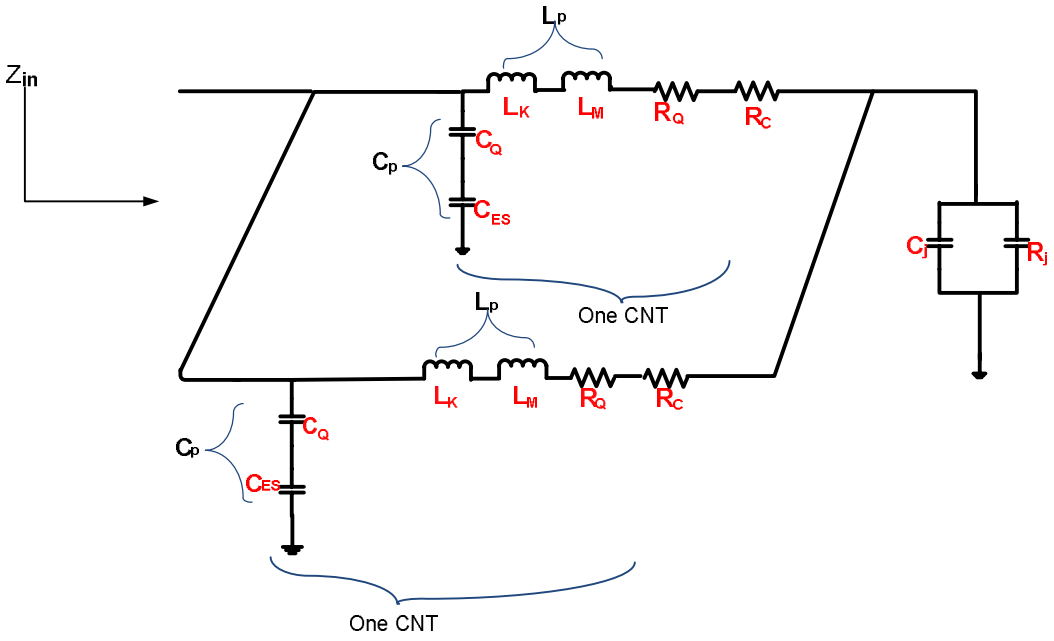

Figure 3.2: Equivalent circuit for two CNTs in parallel across the contacts of a Schottky diode. R_Q corresponds to the 6.45kΩ value that contributes to the series resistance as described in (3.3), where as R_C represents any contact resistance.

The above supposition can be supported by referring back to graphene and making a connection to CNTs. In [29] it is reported that the resistivity of a graphene sheet is equal to $\rho = 6.45\ k\Omega$ (the minimum quantum resistance of a CNT) and the resistance scales as $R = \rho L/w$. From this relationship, as depicted in Figure 3.3, we can see that doubling the width will result in R decreasing by half, tripling the width will reduce the resistance to one third, etc. This corresponds to placing two CNTs in parallel and decreasing the series resistance to one half and three CNTs in parallel leads to reducing the resistance to one third, etc. (see Figure 3.4). We know that if a single sheet of graphene was placed across the two contacts there would be only one R_j that would decrease slightly as the width (area) was increased. Therefore, it is reasonable to assume that as long as the CNTs that are placed in parallel are close enough to one another, a single device, regardless of the number of tubes, will have a single R_j determined by (3.9) and the series resistance will decrease as the junction resistance remains relatively unchanged. The assumption that R_j remains constant is based upon the idea that the area making contact to the CNTs will not increase significantly due to the small nature of the tubes, however in reality I_{sat} probably would increase by some amount and R_j would decrease accordingly. The direct relationship between I_{sat} and the number of tubes is not known at this point, for that reason, the simulations contained within this chapter keep R_j constant with respect to the number of tubes. This would represent a "best case scenario" and even with this assumption we will demonstrate that there are still considerable challenges in making a diode competitive to other non-CNT based devices.

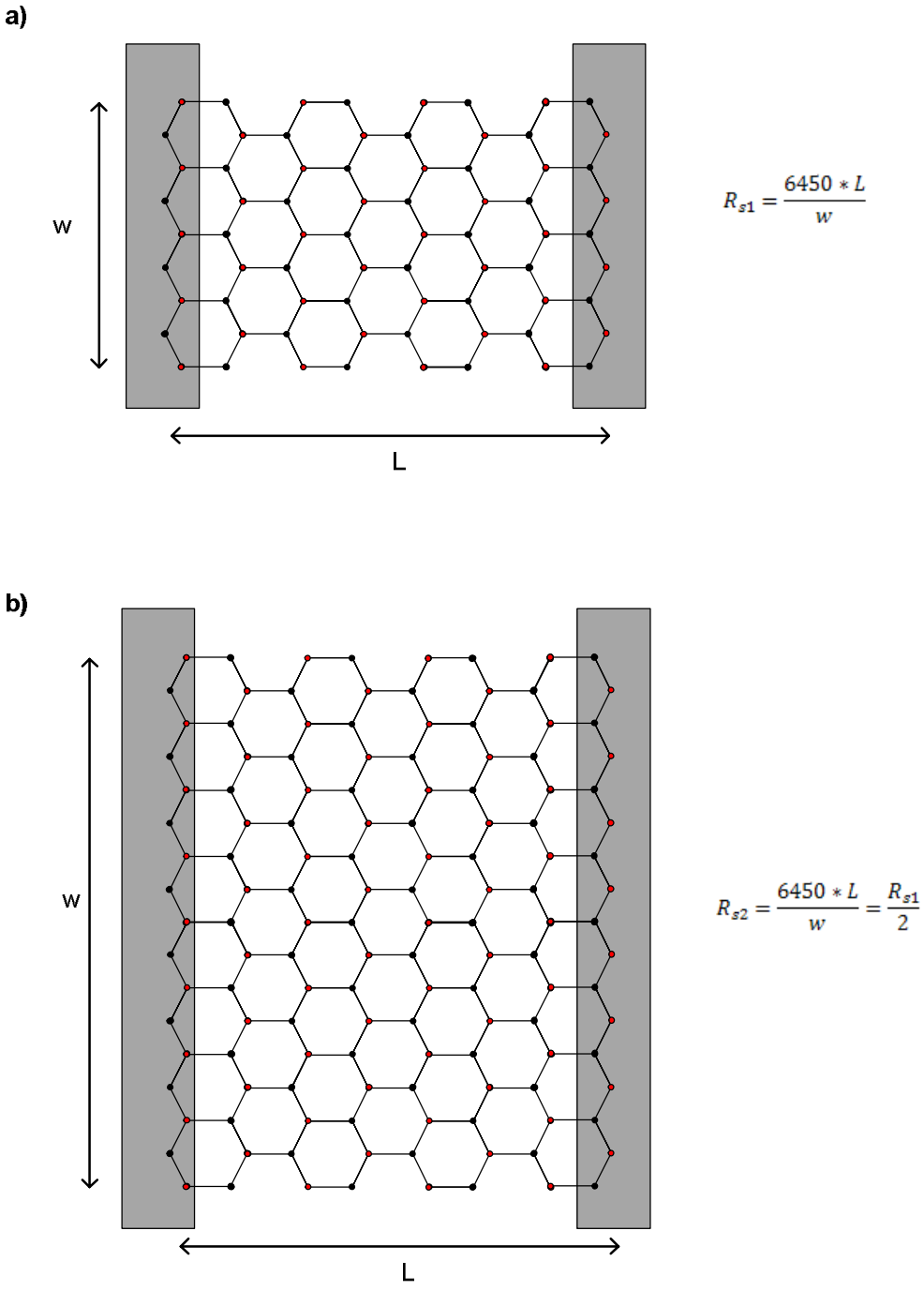

Figure 3.3: (a) Graphene sheet with length L and width w resulting in a series resistance equal to R_{s1}. (b) Graphene sheet with twice the width as (a) and same length with series resistance $R_{s2}=R_{s1}/2$.

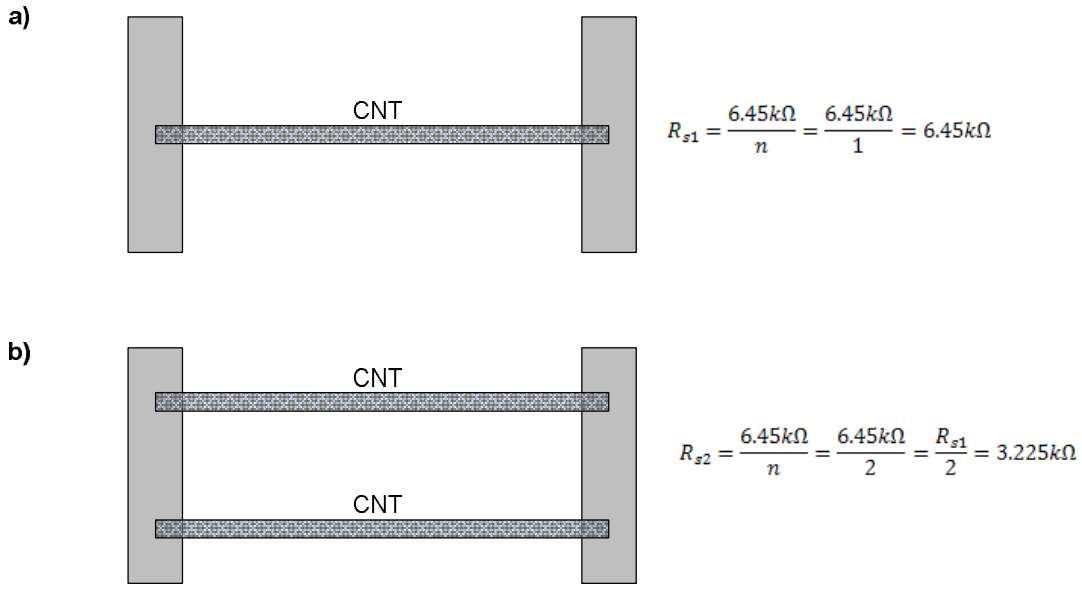

Figure 3.4: a) A single CNT placed across contacts resulting in a series resistance ~6.45kΩ. b) Two closely spaced CNTs in parallel resulting in a series resistance that is reduced by half from the value of (a). The number of tubes is equal to n.

Lumped Element Match to 50 Ohms

In the next three sections we will use the software package, Advanced Design System (ADS) from Agilent Technologies to simulate the matched Schottky diode and speculate whether or not our goal of creating an effective matching network for a CNT-based device is feasible. In the final portion of this chapter we will illustrate the effect of placing several CNTs in parallel in order to improve the percentage of the input power that will be delivered to the load. We will consider two cases at 10GHz as follows:

1) An ideal Schottky diode with perfect contacts assuming we can achieve the maximum conductance so that R_S~6.45kΩ (that is, $R_C = 0$).

2) A Schottky diode with a more realistic value for the conductance through the CNTs ~25% G_o per tube (that is, R_C = 19.35kΩ and R_S = 6.45kΩ).

Then we will determine how adding CNTs in parallel improves the performance of the diode.

Assuming that the lengths of the CNTs are ~2.5μm and the diameters ~1-3nm we calculate the following per nanotube:

$$L_M \approx \frac{1pH}{\mu m} \approx 2.5pH \qquad C_{ES} \approx \frac{50aF}{\mu m} \approx 125aF$$

$$L_K \approx \frac{4nH}{\mu m} \approx 10nH \qquad C_Q \approx \frac{400aF}{\mu m} \approx 1fF$$

$$L_P \approx L_K + L_M \approx 10.003nH \qquad C_P \approx \frac{C_E C_Q}{C_E + C_Q} \approx 111.1aF$$

$R_j = 796\Omega$

$C_j \rightarrow 0F$ (negligible)

The diameters of ~1-3nm were chosen because these are the values most often reported in the literature for these devices. It is important to note that controlling the growth of nanotubes within this range is very reasonable and any variation in the above parameters, due to a 1-2nm difference, is negligible (on the order of ~1% or less). The junction resistance value was obtained from [15], which is an estimated result determined by fitting ideality curves (3.16) to experimental I-V plots.

$$I_o = I_{Sat}\{\exp[q(V_o - IR_S)/(nkT)] - 1\} \tag{3.16}$$

The matching networks for all cases were determined using (3.17) – (3.20) and a generic matching network using these equations is shown in Figure 3.5 [27].

$$B = \frac{X_L - \sqrt{\frac{R_L}{Z_o}}\sqrt{R_L^{\,2} + X_L^{\,2} - Z_o R_L}}{R_L^{\,2} + X_L^{\,2}} \tag{3.17}$$

$$X = \frac{1}{B} + \frac{X_L Z_o}{R_L} - \frac{Z_o}{BR_L} \tag{3.18}$$

$$C_{series} = \frac{1}{|2\pi f X|} \tag{3.19}$$

$$L_{shunt} = \frac{1}{|2\pi f B|} \tag{3.20}$$

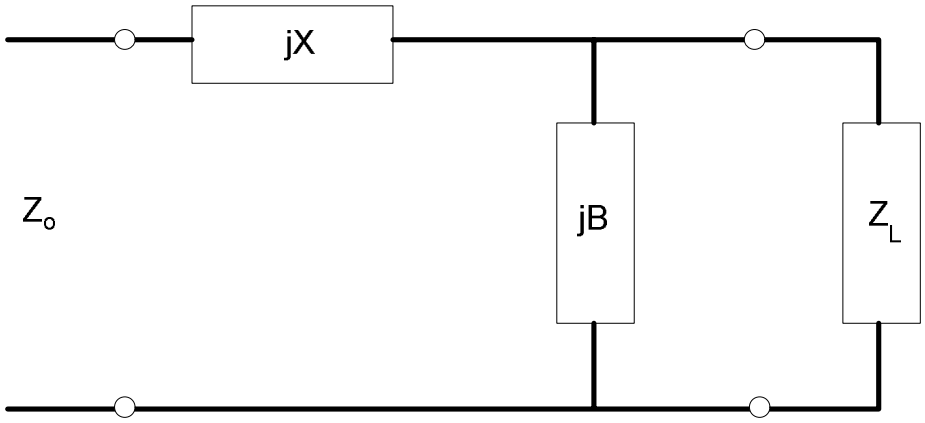

Figure 3.5: Matching Network where Z_L is equal to the impedance calculated in (3.12) and $Z_o = 50\Omega$ [27].

Case I: Ideal Diode with Perfect Contacts (Rs~6.45kΩ) matched at 10 GHz

The simulation completed below (Figures 3.6 and 3.7) illustrate that even for the most ideal case the bandwidth of the successful match is very narrow, approximately a 15dB return loss bandwidth of 300 MHz and a fractional bandwidth equal to 3%, due to the high impedance load. Therefore, we need to operate extremely close to 10 GHz so that we do not have significant power loss.

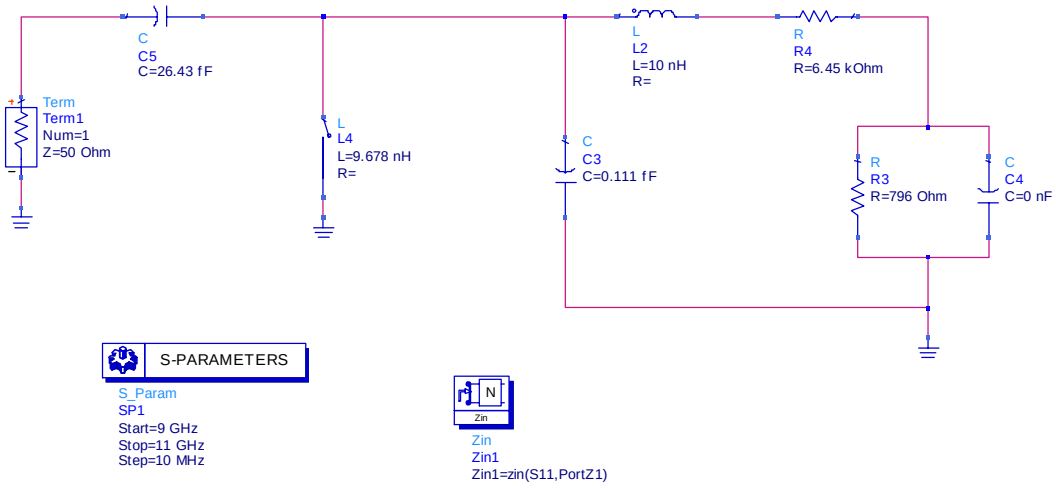

Figure 3.6: Matched Schottky diode at 10 GHz with ideal contacts and one CNT.

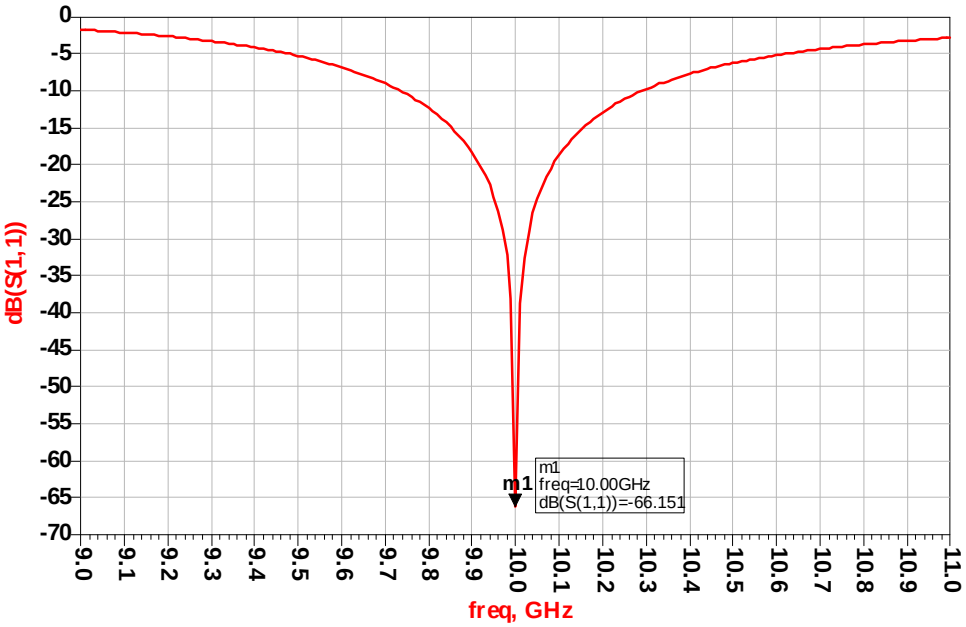

Figure 3.7: Input reflection coefficient of matched Schottky diode with ideal contacts and one CNT (Rs~6.45kΩ).

Case II: Diode with Maximum Conductance per Tube ~25% G_o

Experimentally, the closest semiconducting tubes have come to achieving the maximum allowed conductance is $0.25G_o$. Therefore, we consider this case in order to give a more accurate picture of what may be achieved based on the best available (early 2009) experimental results available in the literature.

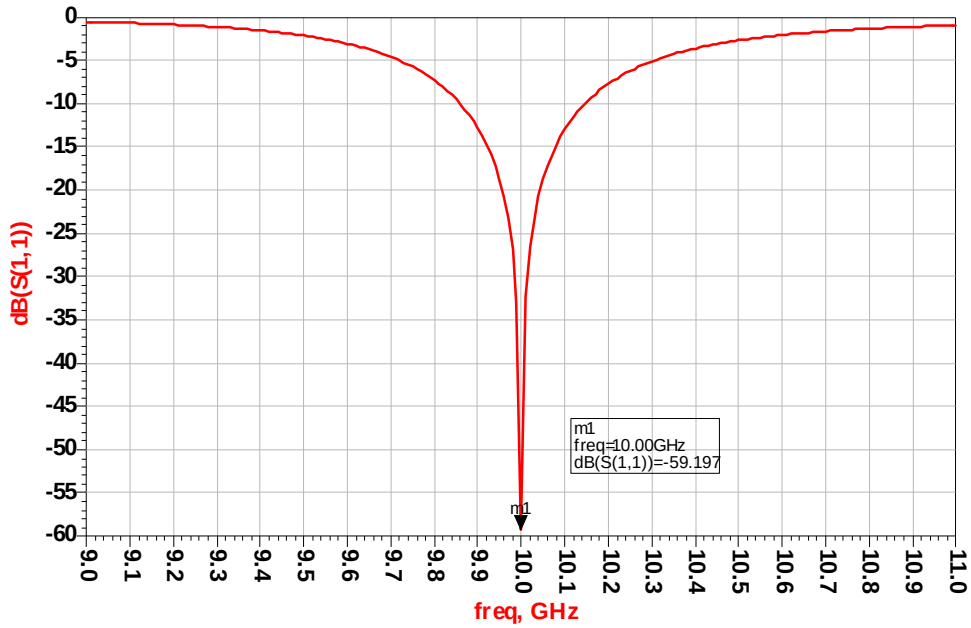

Figure 3.8: Input reflection coefficient of matched Schottky diode with one CNT, ideal contacts and conductance through tube ~25% G_o.

Notice by looking at Figure 3.8 that just as in case I, we have a very narrow bandwidth as expected. A summary of parameter values for the lumped element match is recorded in Table 3.1.

Table 3.1: Parameter Values for Lumped Element Match at 10 GHz (Single CNT)

Case	**R_s** (Ω)	**C_p (fF)**	**L_p (nH)**	**R_j** (Ω)	**C_j (F)**	**C_{series} (fF)**	**L_{shunt} (nH)**	**S_{11} @ 10 GHz**
I	6.45k	0.111	10	796	0	26.43	9.678	-66.151 dB
II	25.8k	0.111	10	796	0	13.81	18.25	-59.197 dB

Shunt Stub Match to 50 Ohms

If we were to implement an on-chip matching network experimentally it would likely be in microstrip and not with lumped elements, therefore, we will now analyze and compare ideal transmission lines to microstrip using a quartz substrate. For this analysis we will compare thick and thin metallization of aluminum in order to determine the effect of the very thin metallization layer that is required for the CNT-based device. The electrical lengths for a single-stub matching network can be determined by the following equations taken from [27]:

$$t = \frac{X_L + \sqrt{\frac{R_L}{Z_o}\left(Z_o - R_L\right)^2 + {X_L}^2}}{R_L - Z_o} \tag{3.20}$$

$$d = \frac{1}{2\pi}\arctan(t) \tag{3.21}$$

$$B = \frac{{R_L}^2 t - \left(Z_o - X_L t\right)\left(X_L + Z_o t\right)}{Z_o\left[{R_L}^2 + \left(X_L + Z_o t\right)^2\right]} \tag{3.22}$$

$$L_{short} = \frac{1}{2\pi}\arctan\left(\frac{Y_o}{B}\right) \tag{3.23}$$

$$Shorted\ Stub\ Length = L_{short} \cdot 360 \tag{3.24}$$

$$Series\ TL\ Length = d \cdot 360 \tag{3.25}$$

Diode with Ideal Transmission Lines at 10 GHz

A summary of component values for matching with ideal transmission lines are given in Table 3.2. Cases I and II are the same as studied in the previous section.

Table 3.2: Parameter Values for Shunt Stub Match with Ideal Transmission Lines at 10 GHz

Case	**R_s** (kΩ)	**C_p (fF)**	**L_p (nH)**	**R_j** (Ω)	**C_j (F)**	**Distance from Load to Stub**	**Stub Length**	**S_{11} @ 10 GHz**
I	6.45k	0.111	10	796	0	85.28º	4.766º	-60.772 dB
II	25.8k	0.111	10	796	0	87.468º	2.52º	-37.371 dB

Microstrip

Finally we will analyze simulations for a shunt stub match using microstrip with a quartz substrate. Currently for the CNT-based Schottky diode only thin contact metallizations on the order of ~nm have been demonstrated (we will consider the case when the metal is aluminum, however other metals such as titanium, gold, or palladium could also be used). We will compare, in simulation, a thicker metallization ~1.5mils to a thin ~100nm in order to understand the extent to which the thinner metallization will negatively impact the effectiveness of our matching network/diode. The relevant properties of a quartz substrate are given in Table 3.3. The LineCalc tool in ADS was

used to determine the widths and lengths of the microstrip sections corresponding to the electrical lengths determined previously.

Table 3.3: Quartz Substrate Information

Dielectric Constant	3.8
Loss Tangent	$1x10^{-4}$
Substrate Thickness	1 mm

Let us consider the same two cases for both a thick metallization layer of aluminum equal to 1.5mils and a thin metallization ~100nm. Note that the conductivity of aluminum is ~$3.767x10^{7}$ (S/m). Tables 3.4 and 3.5 give the widths and lengths of microstrip necessary for our matching network while Table 3.6 compares the input reflection coefficient for each case.

Table 3.4: Case I-Widths and Lengths of Microstrip for the Case of an Ideal Diode with Perfect Contacts and One CNT at 10 GHz

	Shorted Stub	**Series Transmission Line**
Thick Metallization	W= 84.302 mils	W= 84.302 mils
	L= 8.9377 mils	L= 159.9256 mils
Thin Metallization	W= 86.0453 mils	W= 86.0453 mils
	L= 8.8937 mils	L= 159.1386 mils

Table 3.5: Case II-Widths and Lengths of Microstrip for the Case of an Ideal Diode with Perfect Contacts and Maximum Conductance per Tube ~25% G_o (representing recent achievable value recorded experimentally) at 10 GHz

	Shorted Stub	**Series Transmission Line**
Thick Metallization	W= 84.302 mils	W= 84.302 mils
	L= 4.7257 mils	L= 164.0287 mils
Thin Metallization	W= 86.0453 mils	W= 86.0453 mils
	L= 4.70252 mils	L= 1663.2217 mils

Table 3.6: Input Reflection Coefficient Comparison

Case	**R_s** (kΩ)	**C_p (fF)**	**L_p (nH)**	**R_j** (Ω)	**C_j (F)**	**S_{11} @ 10 GHz Thick Metallization**	**S_{11} @10 GHz Thin Metallization**
I	6.45k	0.111	10	796	0	-24.901 dB	-11.009 dB
II	25.8k	0.111	10	796	0	- 15.439 dB	-4.725 dB

We can see from Table 3.6 that the thinner metallization will have a very detrimental impact upon the percentage of the input power that can be delivered to the load. The next section discusses the power output and shows how placing several CNTs in parallel results in significant improvement. However, it does not take into account the effect of the thin metallization necessary for CNTs. Therefore, the percentages given in Tables 3.7 and 3.8 will decrease significantly if we consider the results of Table 3.6, which is a more accurate depiction of an actual device.

Percent of Power Delivered to the Load

Although we can create a matching network to minimize reflection loss as illustrated in the previous section, we must also be concerned about what percentage of the input power will actually be delivered to the load. The following two tables confirm that additional parallel tubes is very advantageous, leading to a potential improvement of 82% from a single tube to 200 tubes. The results assume the realization of lossless matching networks.

Table 3.7: Percent of Input Power Delivered Assuming Perfect Contacts and Conductance per Tube ~G_o (at 10 GHz). In each case, the matching network has been developed to minimize reflection loss.

Number of CNTs Across Contacts	**Percent of Input Power Delivered**
1	11 %
2	19.2 %
3	26 %
5	38.5 %
7	47.5 %
10	54 %
30	75 %
50	85.4 %
75	88.5 %
100	91.2 %
200	93.7 %

Table 3.8: Percent of Input Power Delivered Assuming the Conductance per Tube is ~0.25G_o (at 10 GHz). In each case, the matching network has been developed to minimize reflection loss.

Number of CNTs Across Contacts	**Percent of Input Power Delivered**
1	2.56 %
2	5.8 %
3	8.8 %
5	13.1 %
7	17.2 %
10	23 %
30	41.6 %
50	58.3 %
75	69.8 %
100	75 %
200	81.8 %

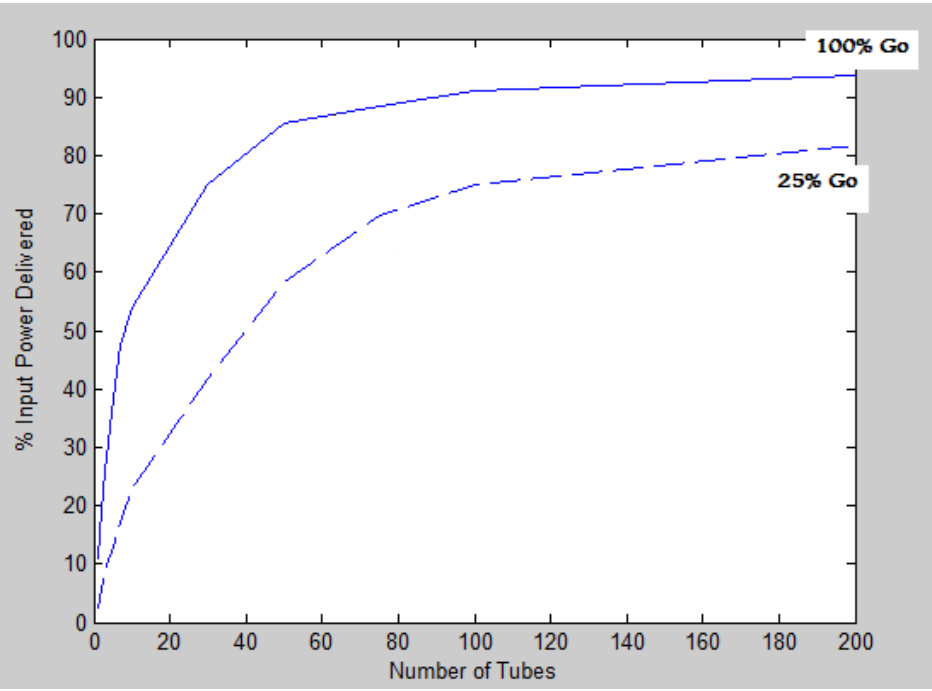

Figure 3.9: Percent of input power delivered vs. the number of CNTs in parallel for the case where the conductance is equal to G_o and 0.25G_o.

Noise Equivalent Power (NEP) and Cutoff Frequency

In this section we will calculate the noise equivalent power and the cutoff frequency for different numbers of tubes across the contacts of the diode. The cutoff frequency can be calculated using (3.26) [15] and is tabulated in Table 3.9 and 3.10 for various numbers of parallel CNTs.

$$f_C = \frac{1}{2\pi R_j C_p}\sqrt{\frac{R_S + R_j}{R_S}} \tag{3.26}$$

Table 3.9: Cutoff Frequency of Schottky Diodes Assuming Perfect Contacts and Conductance per Tube ~G_o (R_j remains a constant 796 Ω).

Number of CNTs Across Contacts	**R_S (Ω)**	**C_p (fF)**	**Cutoff Frequency**
1	6.45k	0.111	1.907 THz
2	3.225k	0.222	1.005 THz
3	2.15k	0.333	702.1 GHz
5	1.29k	0.556	457.7 GHz
7	921	0.778	351 GHz
10	645	1.111	269 GHz
30	215	3.333	130.1 GHz
50	129	5.556	96.37 GHz
75	86	8.333	76.84 GHz
100	64.5	11.111	65.73 GHz
200	32.25	22.222	45.66 GHz

Table 3.10: Cutoff Frequency of Schottky Diodes Assuming the Conductance per Tube is ~$0.25G_o$ (R_j remains a constant 796 Ω).

Number of CNTs Across Contacts	R_S (Ω)	C_p (fF)	Cutoff Frequency
1	25.8k	0.111	1.827 THz
2	12.9k	0.222	927.1 GHz
3	8.6k	0.333	627 GHz
5	5.16k	0.556	386.7 GHz
7	3.686k	0.778	283.5 GHz
10	2.58k	1.111	205.8 GHz
30	860	3.333	83.24 GHz
50	516	5.556	57.396 GHz
75	344	8.333	43.68 GHz
100	258	11.111	36.37 GHz
200	129	22.222	24.09 GHz

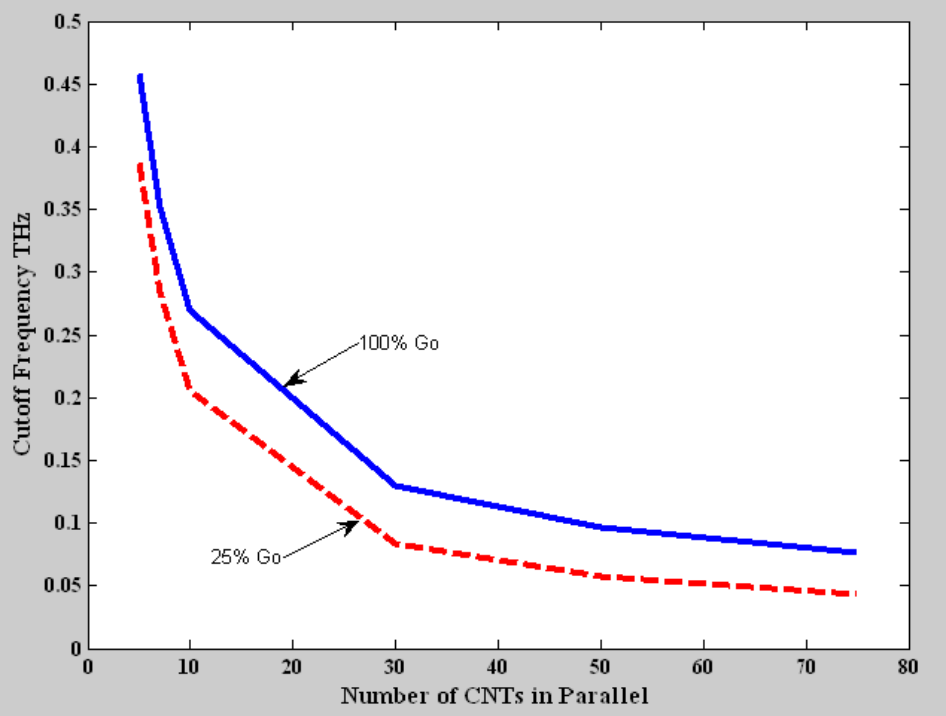

Figure 3.10: Cutoff frequency (f_C) vs. number of CNTs in parallel for the case when the conductance through each tube is 100% Go and 25% Go.

The cutoff frequency initially decreases rapidly as the number of tubes in parallel is increased, but begins to decline much more slowly after about 40-60 tubes have been added (Figure 3.10). Even though the additional parallel CNTs lowers the cutoff frequency significantly we are still theoretically capable of achieving a fairly high value. Therefore, increasing the number of parallel tubes is still very advantageous due to the delivered input power improvement as discussed earlier, though naturally subject to the frequency of interest.

There is one more area of importance we should look at and that is the noise equivalent power (NEP). The NEP is a measure of the sensitivity of a detector (the signal power which gives a signal to noise ratio of one) and it is desirable to have as low as possible in order to achieve a high signal to noise ratio (SNR). Using (3.27) the NEP is calculated for f =10 GHz for the same cases as before. A summary of the results are shown in Tables 3.11 and 3.12.

$$NEP = \frac{2nkT \cdot \sqrt{4kT \cdot \left[\frac{n}{2} R_j + R_S\right]} \cdot \left(1 + \left(\frac{f}{f_C}\right)^2\right)}{qR_j} \tag{3.27}$$

Table 3.11: Noise Equivalent Power (NEP) of Schottky Diodes Assuming the Conductance per Tube is ~G_o with f=10 GHz, R_j=796Ω, n=1.3, and T = 298k.

Number of CNTs Across Contacts	**f_C**	**R_S (Ω)**	**C_p (fF)**	**NEP (W/$\sqrt{Hz}$)**
1	1.907 THz	6.45k	0.111	8.983×10^{-13}
2	1.005 THz	3.225k	0.222	6.584×10^{-13}
3	702.1 GHz	2.15k	0.333	5.559×10^{-13}
5	457.7 GHz	1.29k	0.556	4.577×10^{-13}
7	351 GHz	921	0.778	4.085×10^{-13}
10	269 GHz	645	1.111	3.674×10^{-13}
30	130.1 GHz	215	3.333	2.93×10^{-13}
50	96.37 GHz	129	5.556	2.766×10^{-13}
75	76.84 GHz	86	8.333	2.688×10^{-13}
100	65.73 GHz	64.5	11.111	2.656×10^{-13}
200	45.66 GHz	32.25	22.222	2.644×10^{-13}

Table 3.12: Noise Equivalent Power (NEP) of Schottky Diodes Assuming the Conductance per Tube is ~0.25G_o with f=10 GHz, R_j=796Ω, n=1.3, and T = 298k.

Number of CNTs Across Contacts	**f_C**	**R_S (Ω)**	**C_p (fF)**	**NEP (W/$\sqrt{Hz}$)**
1	1.827 THz	25.8k	0.111	1.746×10^{-12}
2	927.1 GHz	12.9k	0.222	1.247×10^{-12}
3	627 GHz	8.6k	0.333	1.028×10^{-12}
5	386.7 GHz	5.16k	0.556	8.114×10^{-13}
7	283.5 GHz	3.686k	0.778	6.986×10^{-13}
10	205.8 GHz	2.58k	1.111	6.003×10^{-13}
30	83.24 GHz	860	3.333	4.052×10^{-13}
50	57.396 GHz	516	5.556	3.565×10^{-13}
75	43.68 GHz	344	8.333	3.324×10^{-13}
100	36.37 GHz	258	11.111	3.223×10^{-13}
200	24.09 GHz	129	22.222	3.207×10^{-13}

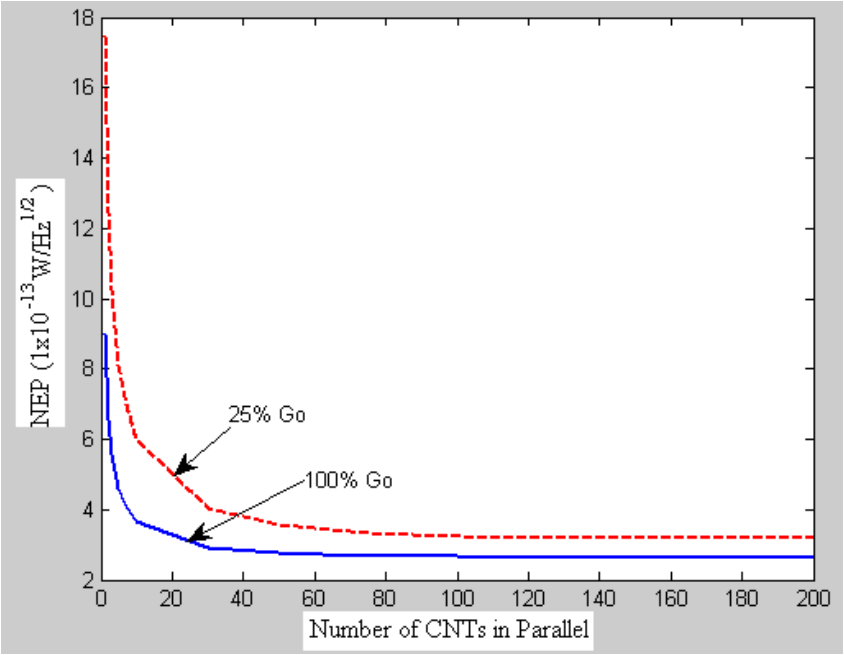

Figure 3.11: Noise equivalent power (NEP) vs. number of CNTs in parallel. The values are calculated for detection at 10 GHz and room temperature assuming the ideality factor of the diodes are n=1.3.

So far we have illustrated that one can significantly improve a CNT-based Schottky diode by adding tubes in parallel across the contacts. However, the enhancement tends to level off after about 200 tubes have been added. This is due to R_s being significantly reduced after 200 have been added and it no longer is as dominate as before. The calculated cutoff frequency for these devices is going to be high due primarily to the very small capacitance C_p, meaning that we can add several tubes in parallel and still observe high cutoff frequencies. An issue of importance is the percentage of the input power that will be successfully delivered. We determined that we can improve the percentage by simultaneously using a matching network to minimize the reflection loss and adding parallel tubes. Although the percentage was high after 100-200 tubes were added we must also consider the effect of the very thin contact metallizations

that so far are the only diodes that have been demonstrated in the literature. The thinner metallization layer is notably detrimental to the amount of power delivered which will be observed for these devices, thus in reality the percentage of the input power delivered even after adding tubes and developing a matching network may be very small.

For comparison Table 3.13 compares a state-of-the-art GaAs diode and a CNT diode.

Table 3.13: Comparison of a CNT based Schottky Diode and a GaAs diode [15].

	CNT Diode (One CNT)	**CNT Diode (200 CNTs)**	**GaAs Diode**
F_C	1.827 THz	24.09 GHz	7 THz
NEP	8.983×10^{-13} W/$\sqrt{Hz}$	2.644×10^{-13} W/$\sqrt{Hz}$	5.4×10^{-13} W/$\sqrt{Hz}$

It is apparent that compared to current state-of-the-art devices, such as GaAs Schottky diodes, the performance of CNT diodes is very poor even when considering the simulated "best case scenario".

In the next section we will look at a CNT-based MOSFET in much the same way we did the diode in order to assess the future potential of such devices.

Carbon Nanotube Transistor Small-Signal Circuit Model

The purpose of this section is to develop an equivalent circuit model for a Schottky barrier FET in a similar manner as the diode model. We will utilize the same concepts to determine the device's quantum capacitance and resistance values. Then investigate the advantages/disadvantages of placing additional tubes in parallel across the

source and drain. Particularly, we will focus on the effect more parallel tubes will have on the cutoff frequency.

The proposed transistor model depicted in Figure 3.13 includes components whose values are determined from experimental results reported in the literature, such as the transconductance g_m and output conductance g_d of the device when it does not behave as an ideal current source, and theoretically calculated values. Let us begin by determining the gate-source capacitance which is equal to the quantum capacitance and electrostatic capacitance in series, the same capacitances determined in the previous chapter for the diode (2.54) and (2.55) [11].

$$C_{gs} \approx \left[\frac{1}{C_E} + \frac{1}{4C_Q} \right]^{-1} \tag{3.28}$$

As before the quantum capacitance is multiplied by four because of the 4-fold degeneracy associated with CNTs.

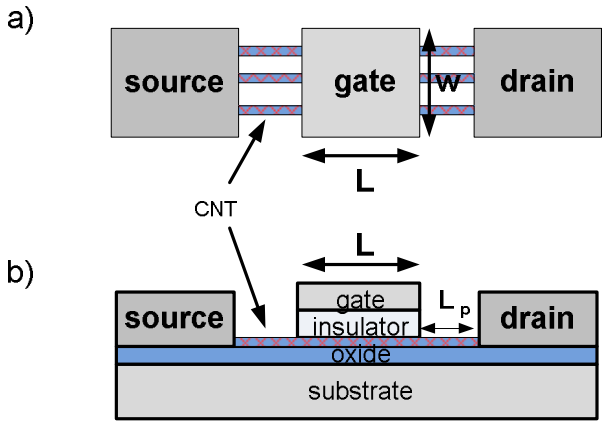

Figure 3.12: a) Top profile of nanotube transistor and b) side profile of a nanotube transistor [11].

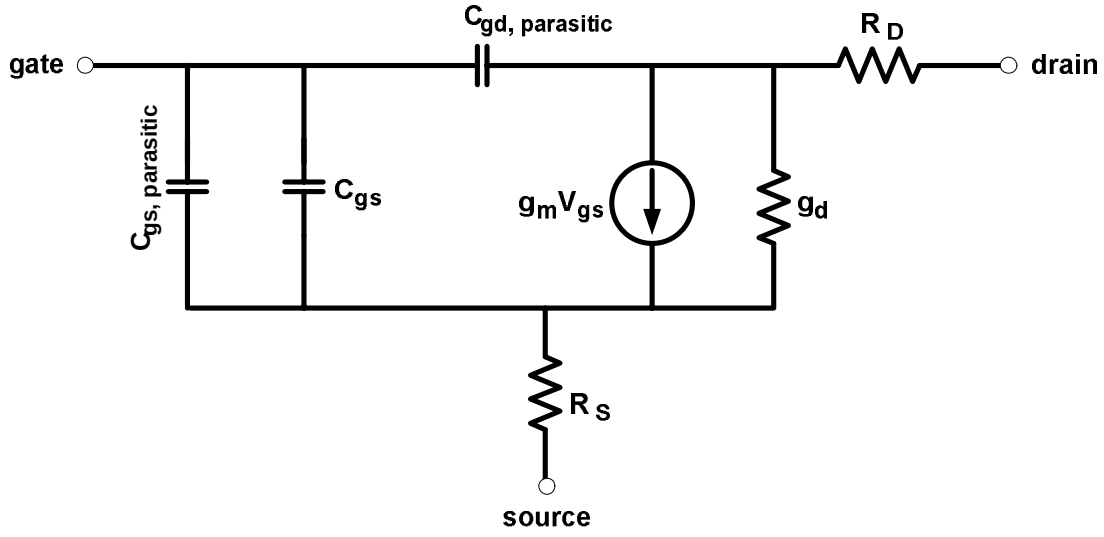

Figure 3.13: Small- signal circuit model for a nanotube transistor [11].

The parasitic capacitances are estimated in [11] using the calculation for what the capacitance would be between two thin metal films separated by a distance L_p. This yields a capacitance equal to ~10^{-16} F per the length of the electrode in μm. For this case the length will be the width of the gate, source or drain as labeled in Figure 3.12 as w. Therefore, assuming the width of the gate electrode is 25 μm, the parasitic capacitances will be close to 2.5 fF.

The series resistances (R_S and R_D) in the transistor model are from the metallization layer and the ohmic contact resistance. Assuming perfect contacts, these resistance values will then be equal to the quantum resistance ~6.45kΩ. The other parameters in Figure 3.13 are determined from experimental values reported in the literature. The following table summarizes a set of values for g_m and g_d taken from the literature.

Table 3.14: Summary of experimental results gathered from recently published journal papers for CNT SBFETS. Note that all CNTs for these devices have diameters between 1-5nm. All values were tabulated by [11] from published I-V curves.

Gate Length	**Gate Thickness**	**g_m**	**g_d (μS)**	**Ref**
0.1 μm	3000 Å	0.3 μS	0.03	[30]
0.3 μm	1000 Å	0.001 μS	1	[31]
1 μm	200 Å	3 μS	<0.1	[32]
3 μm	0 Å	20 μS	<0.1	[33]
1 μm	80 Å	12 μS	<0.1	[34]
10 μm	500 Å	0.05 μS	0.6	[35]
1 μm	10 Å	60 μS	<0.1	[36]
0.3 μm	5000 Å	10 μS	<0.1	[37]

Cutoff Frequency of CNT Transistor

Just as in the previous section we are now going to analyze the cutoff frequency for CNT-based FET for the case when the conductance through a single tube is equal to the fundamental constant G_o and 25%G_o, setting the transconductance to a constant value between each case. We are also going to consider how adding parallel tubes across the source and drain will affect the cutoff frequency of the device. The cutoff frequency can be determined using (3.29) and is defined as the frequency at which the short-circuit current gain drops to unity [11].

$$f_T = \left[2\pi \left((R_S + R_D) C_{gd,parasitic} + \frac{1}{g_m} (C_{gs} + 2C_{gd,parasitic}) + \frac{g_d}{g_m} (R_S + R_D)(C_{gs} + 2C_{gd,parasitic}) \right) \right]^{-1} \tag{3.29}$$

In order to achieve a more reasonable picture of what cutoff frequencies are possible, we will need to consider a few more details. As of today, it is possible to obtain tube densities of ~5 SWNT/μm as reported in [38]. For example, if we set the width to 25 μm the maximum number of parallel CNTs that can be placed across the source and drain is 125. As shown in Figure 3.14, increasing the number of parallel tubes increases the cutoff frequency, but only marginally when compared to the overall picture because decreasing the parasitic capacitance and choosing a smaller gate width improves the cutoff frequency more dramatically. Making the width of the device larger will allow for more tubes, however, the parasitic capacitances will also get larger and begin to lower the cutoff frequency.

Table 3.15: Cutoff Frequency of Schottky Barrier FET Assuming the Conductance per Tube is ~G_o (for tube length 1μm: g_m = 20μs, g_d = 0.1 μs, and parasitic capacitances ~ 10^{-16} F).

Number of Parallel CNTs	**R_S & R_D (Ω)**	**Cutoff Frequency**
1	6.45k	12.42 GHz
2	3.225k	12.72 GHz
3	2.15k	12.82 GHz
5	1.29k	12.9 GHz
7	921.43	12.93 GHz
10	645	12.96 GHz
30	215	13 GHz
50	129	13.01 GHz
75	86	13.01 GHz
100	64.5	13.02 GHz
125	51.6	13.02 GHz

Table 3.16: Cutoff Frequency of Schottky Barrier FET Assuming the Conductance per Tube is ~$0.25G_o$ (for tube length 1µm: g_m = 20µs, g_d = 0.1 µs, and parasitic capacitances ~ 10^{-16} F).

Number of Parallel CNTs	**R_S & R_D (Ω)**	**Cutoff Frequency**
1	25.8k	10.92 GHz
2	12.9k	11.88 GHz
3	8.6k	12.24 GHz
5	5.16k	12.54 GHz
7	3.686k	12.67 GHz
10	2.58k	12.78 GHz
30	860	12.94 GHz
50	516	12.97 GHz
75	344	12.99 GHz
100	258	13 GHz
125	206.4	13 GHz

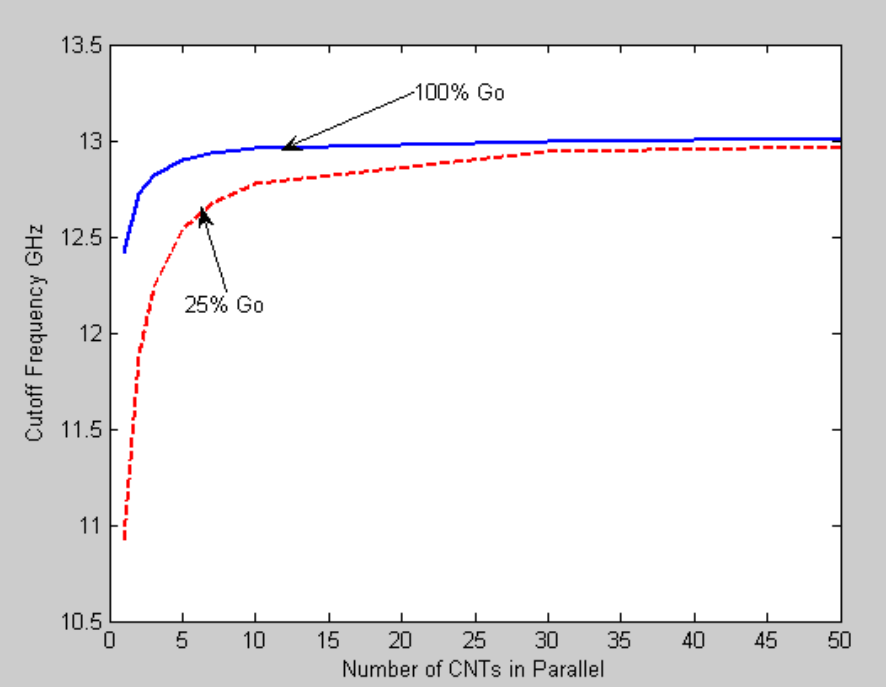

Figure 3.14: Cutoff frequency (GHz) vs. number of CNTs in parallel for a transistor.

In the following two tables only the maximum number of tubes is considered (assuming ~5 SWNT/μm) for variations in the width (w) of the electrodes, taking into consideration the associated increase in the parasitic capacitances in order to estimate the largest potential cutoff frequency for a CNT based FET. In these calculations g_m is set to 20μs. Although g_m is affected by the width (w) it is appropriate in this case to ignore because g_m, C_{gs}, and C_{gd} all increase linearly with increasing w [38]. Thus, as per equation (3.30), the cutoff frequency f_T is independent of w as long as the parasitic resistances are small with respect to the output resistance (due to equation 3.30 only being accurate under this condition).

$$f_T = \frac{g_m}{2\pi\left(C_{gs} + C_{gd}\right)} \tag{3.30}$$

Table 3.17: Cutoff Frequency of Schottky Barrier FET Assuming the Conductance per Tube is ~G_o (for tube length 1μm: g_m = 20μs, g_d = 0.1 μs, and parasitic capacitances varies according to the width of electrodes).

Width (w) (μm)	**Number of Parallel CNTs**	**R_S & R_D (Ω)**	**Parasitic Capacitance (fF)**	**Cutoff Frequency**
1	5	1290	0.1	12.9 GHz
5	25	258	0.5	3.046 GHz
10	50	129	1	1.557 GHz
15	75	86	1.5	1.045 GHz
25	125	51.6	2.5	0.631 GHz
35	175	36.857	3.5	0.4519 GHz
50	250	25.8	5	0.3169 GHz
60	300	21.5	6	0.2643 GHz
80	400	16.125	8	0.1984 GHz
100	500	12.9	10	0.1588 GHz

Table 3.18: Cutoff Frequency of Schottky Barrier FET Assuming the Conductance per Tube is ~$0.25G_o$ (for tube length 1μm: $g_m = 20\mu s$, $g_d = 0.1\ \mu s$, and parasitic capacitances varies according to the width of electrodes).

Width (w) (μm)	**Number of Parallel CNTs**	**R_S & R_D (Ω)**	**Parasitic Capacitance (fF)**	**Cutoff Frequency**
1	5	5160	0.1	12.54 GHz
5	25	1032	0.5	3.042 GHz
10	50	516	1	1.556 GHz
15	75	344	1.5	1.045 GHz
25	125	206.4	2.5	0.6309 GHz
35	175	147.429	3.5	0.4518 GHz
50	250	103.2	5	0.3169 GHz
60	300	86	6	0.2643 GHz
80	400	64.5	8	0.1984 GHz
100	500	51.6	10	0.1588 GHz

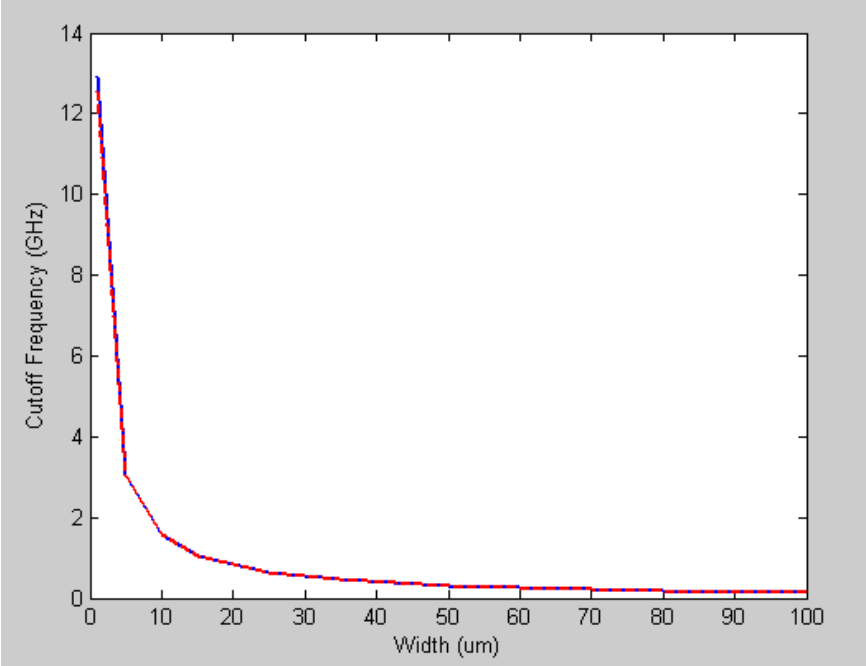

Figure 3.15: Cutoff frequency (GHz) vs. Width (μm) for a transistor assuming density of parallel tubes is 5 per μm.

As one can see from the previous two figures, the increase in the parasitic capacitances due to the larger width is the extremely more dominant factor compared to the parallel tube densities. It is only true that increasing the number of parallel tubes will lead to improvement when the width remains fixed. Otherwise, the effect of larger parasitic capacitances will take over and begin to quickly lower the cutoff frequency regardless of the number of tubes added. To further illustrate this, refer to Table 3.19 where the tube density is set to 20 per μm. These calculations indicate that even with a fairly significant increase in tube density, the results are very similar to the smaller case of 5 per μm. Therefore, choosing the width of the device is more important than the density as well as finding ways to lower the parasitic capacitances.

Table 3.19: Cutoff Frequency of Schottky Barrier FET Assuming the Conductance per Tube is ~G_o and improved tube density of 20 per μm (for tube length 1μm: g_m = 20μs, g_d = 0.1 μs, and parasitic capacitances varies according to the width of electrodes).

Width (w) (μm)	**Number of Parallel CNTs**	**R_S & R_D (Ω)**	**Parasitic Capacitance (fF)**	**Cutoff Frequency**
1	20	322.5	0.1	12.99 GHz
5	100	64.5	0.5	3.047 GHz
10	200	32.25	1	1.557 GHz
15	300	21.5	1.5	1.046 GHz
25	500	12.9	2.5	0.631 GHz
35	700	9.214	3.5	0.4519 GHz
50	1000	6.45	5	0.3169 GHz
60	1200	5.375	6	0.2643 GHz
80	1600	4.031	8	0.1984 GHz
100	2000	3.225	10	0.1588 GHz

The following three figures illustrate more directly how dominate the parasitic capacitances are. In addition to increasing the density of tubes it is possible to raise the

cutoff frequency significantly if the length of the tubes is shortened (decreases C_{gs}) and the parasitic capacitances become negligible. In fact once the parasitics are mitigated and the tube lengths are ~0.05 µm it is possible to achieve cutoff frequencies above 1.8 THz.

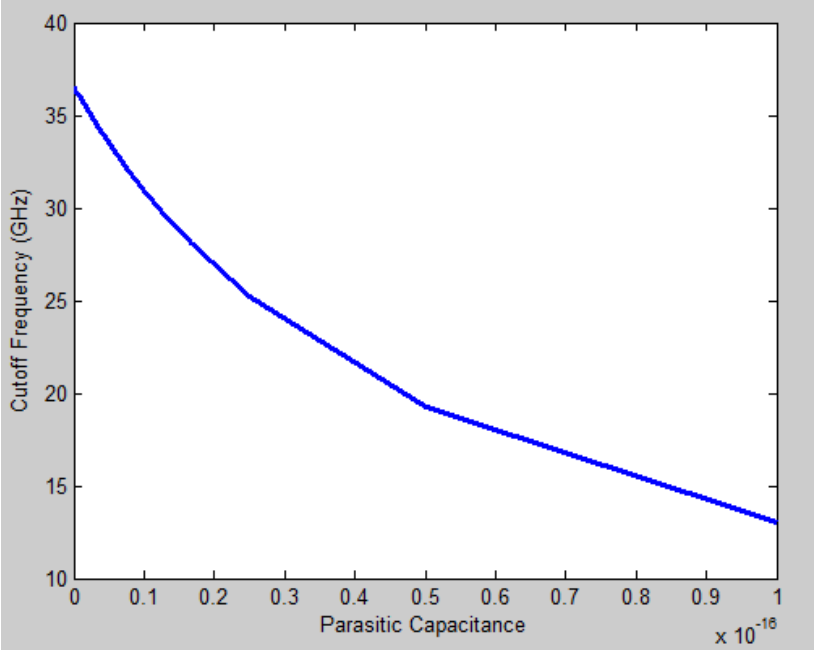

Figure 3.16: Improvement in the cutoff frequency due to decreasing the parasitic capacitance when keeping the number of tubes across the source and drain to 200.

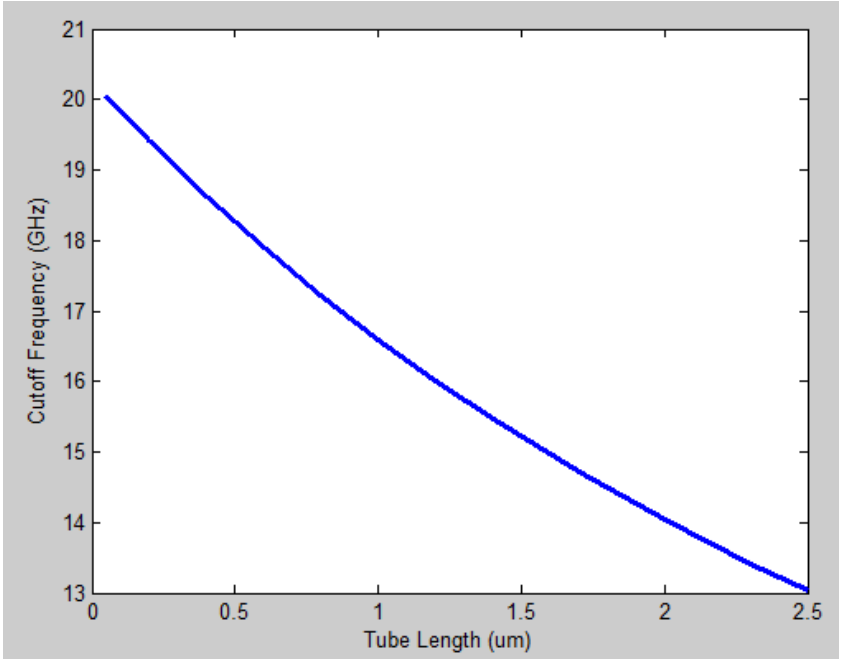

Figure 3.17: Tube length (μm) vs. Cutoff frequency when keeping the parasitic capacitance at 10^{-16} F and 200 tubes across the source and drain.

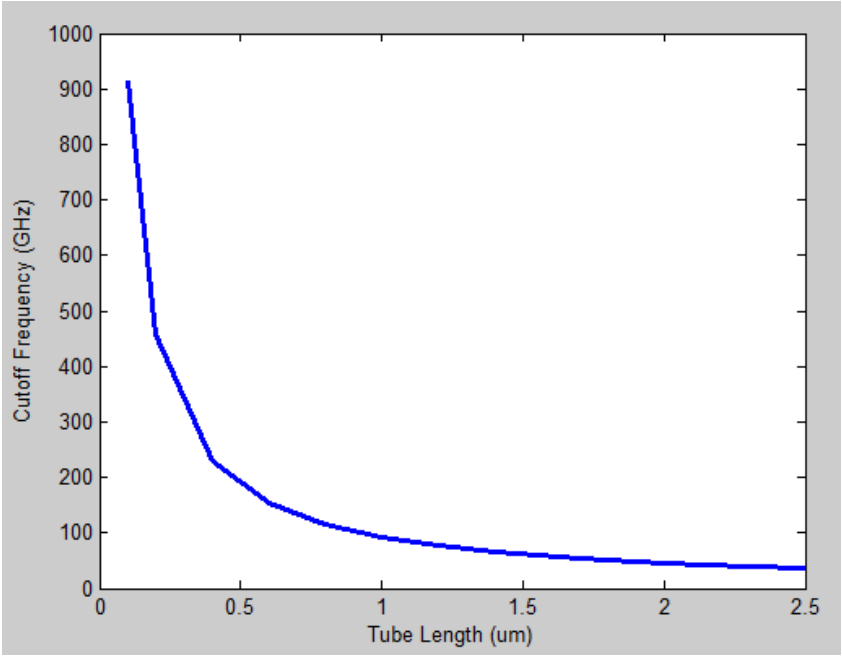

Figure 3.18: Tube length (μm) vs. Cutoff frequency assuming parasitic capacitances are negligible.

Summary

In this chapter we have illustrated through a set of equivalent circuit models and simulations some of the potential advantages and disadvantages of carbon nanotube based devices. These simulations corroborate with the most recent information available in the literature, which includes some experimental data. Theoretically, it is believed that CNT based devices may reach cutoff frequencies in the THz regime and currently most experimental results yield frequencies between 5-9 GHz [38]. Improving these devices will involve improvements in the fabrication processes which will produce higher yield and allow higher density of parallel tubes to be grown in a precise manner. However, even given the "best case scenario" assuming there is no limitations on performance arising due to fabrication limitations, there are still considerable problems associated with CNT based devices for high frequency applications. For example, there is a trade-off with regards to improving the performance of the Schottky diode. Although a higher density of tubes across the contacts will improve power delivery, the cutoff frequency will simultaneously decrease with each additional tube. Also, the parasitic capacitances will need to be lowered virtually to zero in order to achieve cutoff frequencies in the THz regime. This paints a rather grim picture with regards to these devices competing to what is already commercially available.

CONCLUSION

Carbon nanotubes may not be as promising for device applications in high frequency nanoelectronics as initially predicted. There are unfavorable consequences related to the 1-dimensional nature of carbon nanotubes that make it difficult for them to compete with CMOS for millimeter/submillimeter wave nanoelectronics. To date there have been several theoretical and experimental studies made toward determining both the future potential these devices may have as well as the current challenges faced in realizing their full potential. This thesis has covered the development of equivalent circuit models for a Schottky barrier FET and diode and has shown the effect and benefits in incorporating several parallel tubes in these devices. Although they may not be extremely promising for high frequency electronics, their combined mechanical and electrical properties do point to them being better suited for other applications.

One of the main issues still detrimental to CNT based electronics is that it has not yet been demonstrated how well they can be created reliably in a repeatable manner. The literature suggests poor yield when fabricating several of these devices. This is the main factor that needs to be improved first because it is this limitation that will prevent nanotubes from being used even for applications other than high frequency devices.

Future Work

The suggested focus for future work is primarily centered on validating the equivalent circuit models discussed in this thesis with experiment. In particular, one should fabricate both Schottky diodes and FETs with various geometries and aligned

parallel tube densities in order to further support the findings in Chapter 3. There is also a need to create several devices that have the same geometry and tube densities in order to determine if they all behave similarly. In other words, can one control reliably how these devices behave by setting the geometry and number of tubes, or do other factors play a role that cannot easily be controlled, such as the variability in chirality between tubes? Consequently this brings the fundamental challenge with CNTs back to how the growth of tubes can be improved such that chirality can be more readily controlled. The answer to whether this can be accomplished will largely determine the future prospects of carbon nanotube based electronics.

REFERENCES CITED

1. M. Monthioux and V. L. Kuznetsov, “Who should be given the credit for the discovery of carbon nanotubes?” Carbon 44 (2006) 1621-1623.

2. P. J. F. Harris, *Carbon Nanotubes and Related Structures: New Materials for the Twenty-first Century*. Cambridge; New York: Cambridge University Press, 1999.

3. R. Martel, T. Schmidt, H. R. Shea, T. Hertel, and Ph. Avouris, Appl. Phys. Lett. **73**, 2447 (1998).

4. S. Bandow, S. Asaka, Y. Saito, A.M. Rao, L. Grigorian, E. Richter, and P.C. Eklund, Phys. Rev. Lett. **80**, 3779 (1998).

5. M. Meyyappan, *Carbon Nanotubes: Science and Applications*. CRC Press, 2005.

6. J. Zhao, J. Han, and J. Ping Lu, Phys. Rev. B, Vol. 65, 193401 (2002).

7. M. S. Dresselhaus, G. Dresselhaus, and R. Saito, "Physics of carbon nanotubes", *Carbon*, **33**, 883 (1995).

8. M. S. Dresselhaus, G. Dresselhaus, and P. C. Eklund, “*Science of fullerenes and carbon nanotubes*", Academic Press, San Diego, 1996.

9. C. Kocabas, S. Kang, T. Ozel, M. Shim, and J. Rogers, “Improved Synthesis of Aligned Arrays of Single-Walled Carbon Nanotubes and Their Implementation in Thin Film Type Transistors”. *J. Phys. Chem.*, 111, 17879-17886 (2007).

10. J. Kong, H. T. Soh, A. M. Cassell, C. F. Quate, and H. Dai, “Synthesis of individual single-walled carbon nanotubes on patterned silicon wafers”. *Nature*, Vol. 395, Oct. 29 (1998).

11. P. J. Burke, “AC Performance of Nanoelectronics: Towards a Ballistic THz Nanotube Transistor”. *Solid-State Electronics*, 48 (2004).

12. S. O. Kasap, *Principles of Electronic Materials and Devices*. McGraw Hill, 2006.

13. B. G. Streetman and S. K. Banerjee, *Solid State Electronic Devices*. Prentice Hall, Upper Saddle River, New Jersey, 2006.

14. Y. Nosho, Y. Ohno, S. Kishimoto, and T. Mizutani, “Relation between Conduction Property and Work Function of Contact Metal in Carbon Nanotube Field-Effect Transistors”. *Nanotechnology*, 17 (2006).

15. H. Manohara, E. W. Wong, E. Schlecht, B. D. Hunt, and P. H. Siegel, "Carbon Nanotube Schottky Diodes Using Ti-Schottky and Pt-Ohmic Contacts for High Frequency Applications," Nano Lett. Vol. 5, No. 7 (2005).

16. D. Abdula and M. Shim, "Performance and Photovoltaic Response of Polymer-Doped Carbon Nanotube p-n Diodes," ACS NANO Vol. 2, No. 10 (2008).

17. S. J. Wind, J. Appenzeller, and Ph. Avouris, "Lateral Scaling in Carbon-Nanotube Field-Effect Transistors". *Physical Review Letters*, 91 (2003).

18. O. Brand, G. K. Fedder, C. Hierold, J. G. Korvink, and O. Tabata, *Carbon Nanotube Devices: Properties, Modeling, Integration and Applications.* WILEY-VCH Verlag GmbH & Co. KGaA, Weinheim, 2008.

19. S. Datta, *Quantum Transport: Atom to Transistor*. Cambridge University Press, 2006.

20. R. Saito, G. Dresselhaus, and M. S. Dresselhaus, *Physical Properties of Carbon Nanotubes.* Imperial College Press, 2005.

21. A. Loiseau, P. Launois, P. Petit, S. Roche, and J.-P. Salvetat, *Understanding Carbon Nanotubes: From Basics to Applications*, Lect. Notes Phys. 677 (Springer, Berlin Heidelberg 2006).

22. Kotz, Treichel, and Weaver, *Chemistry & Chemical Reactivity 6th ed.*, Brooks/Cole, a division of Thomson Learning, Inc., 2006.

23. P. R. Wallace, "The band theory of graphite," Phys. Rev., **71** (1947) 622-634.

24. A. Jorio, G. Dresselhaus, M. Dresselhaus, *Carbon Nanotubes: Advanced Topics in in the Synthesis, Structure, Properties and Applications*, Topics in Applied Phys. 111 (Springer, 2008).

25. G. Pennington and N. Goldsman, "Modeling Semiconductor Carbon Nanotube Rectifying Heterojunctions," Simulation of Semiconductor Processes and Devices 2001: SISPAD 01, 218 (Springer, 2001).

26. P. J. Burke, "Lüttinger Liquid Theory as a Model of the Gigahertz Electrical Properties of Carbon Nanotubes". *IEEE Trans. On Nanotechnology*, Vol. 1, No. 3 (2002).

27. D. M. Pozar, *Microwave Engineering 3rd Ed*. John Wiley & Sons, Inc., 2005.

28. B. L. Anderson and R. L. Anderson, *Fundamentals of Semiconductor Devices*. McGraw Hill, New York, NY 2005.

29. K. S. Novoselov, A. K. Geim, S. V. Morozov, D. Jiang, M. I. Katsnelson, I.V. Grigorieva, S. V. Dubonos and A. A. Firsov. "Two-dimensional gas of massless Dirac fermions in grapheme," Nature Vol. 438, Nov. 2005.

30. Tans S, Verschueren A, Dekker C. "Room-Temperature Transistor Based on a Single Carbon Nanotube," Nature 1998, 393 (49-52).

31. Martel R, Schmidt T, Shea HR, Hertel T, Avouris Ph, "Single- and Multi-wall Carbon Nanotube Field-Effect Transistors," Appl Phys. Lett. 73(17) 1998: 2447-9.

32. Wind SJ, Appenzeller J, Martel R, Derycke V, Avouris Ph. "Vertical Scaling of Carbon Nanotube Field-Effect Transistors using Top Gate Electrodes," Appl. Phys. Lett. 80(20) 2002: 3817-9.

33. Rosenblatt S, Yaish Y, Park J, Gore J, Sazonov V, McEuen PL, "High Performance Electrolyte Gated Carbon Nanotube Transistors," Nano Lett 2(8) 2002: 869-72.

34. Javey A, Kim H, Brink M, Wang Q, Ural A, Guo J, Mcintyre P, McEuen P, Lundstrom M, Dai H. "High-K Dielectrics for Advanced Carbon-Nanotube Transistors and Logic Gates," Nature Mater 2002 (1): 241-6.

35. Li S, Yu Z, Burke P. "Silicon Nitride Gate Dielectric for Top Gated Carbon Nanotube Transistors," J. Vac. Sci. Technol. B 22(6), Dec. 2004.

36. Guo J, Lundstrom M, Datta S. "Performance Projections for Ballistic Carbon Nanotube Field-Effect Transistors," Appl Phys. Lett. 60 (17) 2002: 3192-4.

37. Javey A, Guo J, Wang Q, Lundstrom M, Dai H. "Ballistic Carbon Nanotube Field-Effect Transistors," Nature 424, 2002: 654-7.

38. C. Kocabas, S. Dunham, Q. Cao, K. Cimino, X. Ho, H. Kim, D. Dawson, J. Payne, M. Stuenkel, H. Zhang, T. Banks, M. Feng, S. V. Rotkin, and J. A. Rogers, "High-Frequency Performance of Submicrometer Transistors that Use Aligned Arrays of Single-Walled Carbon Nanotubes." *Nano Lett.*, 9 (5), 2009, 1937-1943.